Journal of Wind Engineering & Industrial Aerodynamics 172 (2018) 379–394

Contents lists available at ScienceDirect

Journal of Wind Engineering & Industrial Aerodynamics

journal homepage: www.elsevier.com/locate/jweia

An experimental investigation on the aeromechanics and wake interferences of wind turbines sited over complex terrain

Wei Tian [a,b], Ahmet Ozbay [b], Hui Hu [b,*]

[a] School of Aeronautics and Astronautics, Shanghai Jiao Tong University, Shanghai 200240, China
[b] Department of Aerospace Engineering, Iowa State University, Ames, IA 50010, USA

ARTICLE INFO

Keywords:
Wind turbine
Complex terrain
Wake interferences
Atmospheric boundary layer wind
Wind tunnel experiment

ABSTRACT

An experimental study was conducted to investigate the aeromechanics and wake interferences of wind turbines sited on two-dimensional hills with different slopes. First, detailed flow field measurements were correlated with dynamic wind load measurements to reveal the effect of topography on the performance of an individual wind turbine sited at different locations on hilly terrains. Compared to a flat surface, wind turbines sited on a hilltop not only generate more power due to the speed-up effect but also experience reduced fatigue loads due to the decreased level of the turbulence on a hilltop. It was also found that a wind turbine located downstream of a steep hill has a greater likelihood of experiencing extreme wind loads compared to one on a gentle hill. Second, wind turbine wake characteristics and their effects on the dynamic wind loads of downstream wind turbines were also assessed. The effect of an upstream turbine wake on the wind turbine sited on a hilltop was found to be much less significant compared to a wind turbine on a flat surface. In addition, while the wake of an upstream turbine sited on hilltop has a significant influence on the dynamic wind loads of a downstream turbine sited behind a gentle hill, the effect of an upstream turbine wake on a downstream turbine placed behind a steep hill was found to be almost negligible. The quantitative measurement results of the present study not only provide a database for the validation of wake models and numerical simulations but can also be used to optimize the layout of wind turbines sited on complex terrain for higher power yield and better durability.

1. Introduction

Wind energy, as a renewable and clean energy source, has received increased attention in recent years due to its vast potential and availability. With the rapid increase of installed wind energy capacity, the exploitation of additional areas with high wind potential is one of the most important challenges faced by the entire wind energy community. The considerable heights of most rolling hills in complex terrains tend to increase the mean wind velocities due to the speed-up effects. Numerous wind farms in the planning stages are to be located in complex terrains. However, complex terrains also induce negative influences due to the increased turbulence level, high wind shear and flow separation. Therefore, in order to utilize the high mean wind speeds to increase the power production while avoiding the negative influences, the understanding of detailed surface wind characteristics over complex terrains and the optimum micro-siting design of wind farms sited in complex terrains are greatly desired.

It is known that complex terrains have a significant influence on the local wind environment, including wind speed, wind direction, and wind turbulence. These parameters are all highly affected by the local topography, and they usually change significantly over a short distance. Many studies related to the turbulent flow over complex terrains have been performed since the 1970s. Taylor and Gent (1974) and Jackson and Hunt (1975) presented analytical solutions to model the turbulent flow over two-dimensional, smooth hills. Their theories were then extended by many other researchers, including Mason and Sykes (1979), Bradley (1980) and Hunt et al. (1988a, 1988b). Mason and Sykes (1979) developed an analytical solution for three-dimensional topography that become the basis for the models developed by Walmsley et al. (1982) and Taylor et al. (1983). The rapid distortion theory was introduced by Britter et al. (1981) to estimate the change in turbulent properties of the flow over hills. An important feature of flow over hills is the speed-up effect. The speed-up effect along the upstream slope of the hill is mainly dominated by the pressure gradient along the streamline. This pressure gradient was found to be highly related to the hill slope, which has been demonstrated by several theories (Jackson and Hunt, 1975;

* Corresponding author.
E-mail address: huhui@iastate.edu (H. Hu).

https://doi.org/10.1016/j.jweia.2017.11.018
Received 13 June 2016; Received in revised form 18 November 2017; Accepted 18 November 2017

Hunt et al., 1988a). By applying linear theory to a gentle hill, Jackson and Hunt (1975) predicted that the speed-up at the hilltop is approximately proportional to the hill slope. Later, Lemelin et al. (1988) proposed a simple empirical model to estimate the wind speed-up based on computational and wind tunnel data obtained for various shapes of hills. By utilizing computational fluid dynamic (CFD) with the $k-\varepsilon$ turbulence model, Paterson and Holmes (1993) established the values of topographic multipliers to estimate the wind speed-up over hills. Miller and Davenport (1998) quantified the effect of topography and compared the observed speed-ups with those predicted by the Canadian and UK wind loading codes. Weng et al. (2000) incorporated the effects of surface roughness and non-linearity on the fractional speed-up over hilly terrains. Pellegrini and Bodstein (2004) proposed a new analytically-derived expression to predict the height of the maximum speed-up for atmospheric boundary layer (ABL) flows over low hills. A CFD trained neural network for computing the speed-up ratio for flow over hills was introduced in the studies of Bitsuamlak et al. (2006, 2007). Finnigan and Belcher (2004) and Harman and Finnigan (2010) develop an analytical model for ABL flow over a hill that is covered with a vegetation canopy. They indicated that the perturbations to the flow within the canopy are driven by the pressure gradient associated with the flow over the hill. In addition, a majority of the CFD studies were performed by means of the Reynolds-Averaged Navier-Stokes equations (RANS) and Large Eddy Simulation (LES) (Bowen, 2003; Uchida and Ohya, 2003; Bechmann and Sørensen, 2011; Balogh et al., 2012). In addition to these theoretical and CFD studies, numerous wind tunnel experiments and field measurements have been also performed. Britter et al. (1981) measured the stream-wise velocity over a bell-shaped, two-dimensional hill placed in a neutrally stratified boundary layer. The results agree well with the model proposed by Jackson and Hunt (1975). Furthermore, Coppin et al. (1994) investigated the flow field over Cooper's Ridge for various atmospheric stability conditions, and found that the speed-ups over the ridge show significant differences between neutral and non-neutral conditions. Lubitz and White (2007) found that wind speed-up could vary significantly depending on the approaching wind direction.

In comparison to the flow characteristics on a gentle hill, the behavior of the mean and turbulent characteristics of the flow on the lee side of a steep hill fundamentally differ due to the flow separation. A number of experimental and numerical studies were conducted to better understand the flow characteristics over steep hills. Ferreira et al. (1991, 1995) studied the turbulent isothermal flow around two-dimensional sinusoidal hills and indicated that the extension of the recirculating region was strongly dependent on the hill shapes. Kim et al. (1997) compared the low Reynolds number model with the $k-\varepsilon$ model and found that the former predicted the flow separation on the lee side of a steep hill much better. Ying and Canuto (1997) numerically studied turbulent flow over two-dimensional hills and proposed a second-order closure model which accounts for advection, diffusion, production and dissipation processes to represent the Reynolds stresses distribution over hills. Carpenter and Locke (1999) performed a wind tunnel study of the flow over a variety of hill geometries and compared mean speeds with the results calculated using CFD. Athanassiadou and Castro (2001) investigated neutral flow over a series of sinusoidal hills and compared the results with linear theory predictions for the flow in the inner region and aloft. Cao and Tamura (2006) indicated that the surface roughness increases the speed-up ratio above the crest. Later, Cao and Tamura (2007) studied the effects of sudden changes in roughness on the turbulent flow over a steep hill, and found that the speed-up ratio depends strongly on the surface conditions in the middle layer, with the inviscid but rotational part of the outer layer defined by Hunt et al. (1988a). Røkenes and Krogstad (2009) experimentally demonstrated that even for the hill models with steep slope, the speed-up of the flow on the hilltops still approximately has a proportional relationship with average slope of the hill. These studies have given insight into the turbulent flow over hills, and the related data have been embodied in numerous wind loading codes (AIJ, 1996; ASCE, 2002, 2005, 2010; AS/NZ1170.2, 2002; CEN, 2004). This foundation enables us to further explore the effects of mean and turbulent flow characteristics on the performances of wind turbines placed at different locations over a hill.

In addition, the interaction among turbine arrays in a large wind farm is an important aspect that needs to be considered because it reduces power generation and creates higher fatigue loads for the wind turbines experiencing wake flow compared to the upstream turbines under free-stream conditions. The turbine wake is characterized by a substantial stream-wise velocity deficit, which leads to less available wind energy for the downstream turbines to harvest. It also causes enhanced turbulence intensity, which increases the fatigue loads acting on the downstream turbines. It has been found that the power generation of a wind turbine could be reduced by up to 40% when the wind turbine operates within the wake of an array rather than within free-stream flow (Corten et al., 2004). The enhanced turbulence intensity can dramatically shorten the lifetime of the wind turbine (Van Binh et al., 2008; Sanderse, 2009). One area of focus in wind farm design is to develop robust wake models with various atmosphere conditions. However, most of these studies are related to flat surfaces. Barthelmie et al. (2007) and Politis et al. (2012) attempted to evaluate the performance of those models and to examine the evolution of turbine wakes over complex terrains. They found that those wake models could not be used to accurately predict the wake interference in wind farms on complex terrains. The challenges associated with the development of wake models for wind farms sited on complex terrains are that there have been few quantitative measurements on the wake interferences of the wind turbines sited over complex terrains.

In the present study, the flow characteristics of the surface wind over two-dimensional hills with different slopes were studied to assess the characteristics of surface wind energy resources over hilly terrains. The dynamic forces acting on the model wind turbines mounted at different positions on hilly terrains were also measured. The quantitative flow field measurements were correlated with the wind load measurements to investigate the effects of topography on the performance of the wind turbines sited on hilly terrains. In addition, the wake interferences of wind turbines sited on hilly terrains were assessed. The quantitative measurement results of the present study can not only be used as a database for the development of wake models and numerical simulations, but can also be used in designing the optimal layout of wind farms located in complex terrains.

2. Experimental setup

2.1. Atmospheric boundary layer wind tunnel

Experimental studies were performed in a large-scale ABL wind tunnel located at the Aerospace Engineering Department of Iowa State University. Fig. 1(a) shows a sketch of the ABL wind tunnel. The wind tunnel has a contraction section with a 4.8:1 area ratio upstream of the test section along with a set of honeycombs, wire meshes, and a cooling system to provide uniform airflow into the test section. The wind tunnel is operated as a closed return loop. The test section is 20 m long, 2.4 m wide and 2.3 m high. The maximum wind speed is 45 m/s in the test section. During the experiments, the triangular spires at the beginning of the test section and wooden blocks spaced on the wind tunnel floor were used to simulate the flow conditions similar to ABL wind under thermally neutral conditions. As shown in Fig. 1(b), five spires with aspect ratio of 0.16 are equally distributed at the beginning of the test section, on a plane normal to the flow direction. A thin plate with the height of 200 mm are mounted on the wind tunnel floor and connected with the five spires. In addition, surface roughness elements with different size and spacing are covered on the wind tunnel floor. The parameters of the surface roughness elements are listed in Table 1.

In the present study, Cobra Probe anemometry was used to characterize the ABL inflow condition. Mean velocities and turbulent

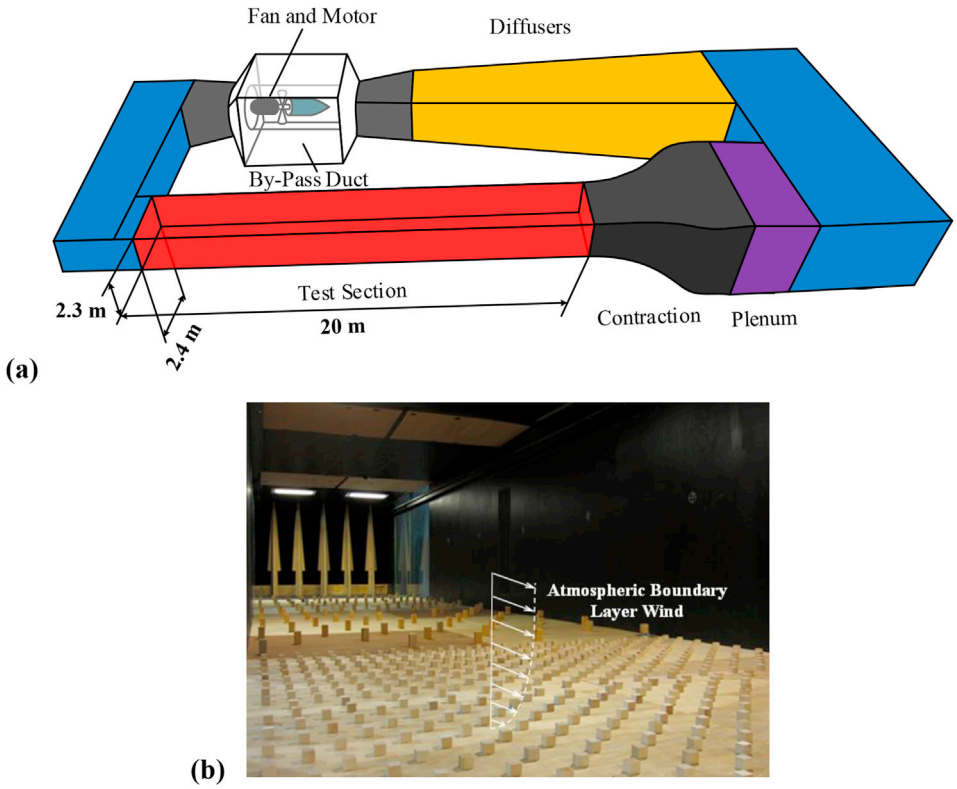

Fig. 1. ABL wind tunnel (a) A sketch of the wind tunnel and (b) A picture of the test section.

Table 1
The parameters of the surface roughness elements.

Roughness elements	Height	Length	Width	Stream-wise spacing	Span-wise spacing	Layout
Dimension (mm)	50.8	38.1	38.1	381	190.5	Staggered
	25.4	25.4	25.4	152.4	152.4	Staggered
	12.7	12.7	12.7	101.6	101.6	Staggered
	6.35	6.35	6.35	50.8	50.8	Staggered

fluctuations of the ABL inflow were measured in three spatial directions before the hill and wind turbine models were installed. Measurements were taken at the centerline of the wind tunnel in the transverse direction and at a fixed stream-wise location (i.e., where the tested wind turbine model will be installed) with the vertical coordinate ranging from $z = 12.7$ to 762 *mm* with an increment of 12.7 *mm* between 12.7 *mm* $\leq z \leq$ 381 *mm* and an increment of 25.4 *mm* in the range of 381 *mm* $\leq z \leq$ 762 *mm*. During the experiments, the oncoming ABL wind speed at hub height of the model wind turbine was kept constant and set as $U_{Hub} = 5.0$ *m*/s. It has been suggested that the mean velocity profile of ABL wind over open terrain can usually be fitted well by a power function or a logarithmic function (Zhou and Kareem, 2002; Jain, 2007). Fig. 2(a) shows the measured mean stream-wise velocity profile of the simulated oncoming ABL wind in the wind tunnel test section. The horizontal axis

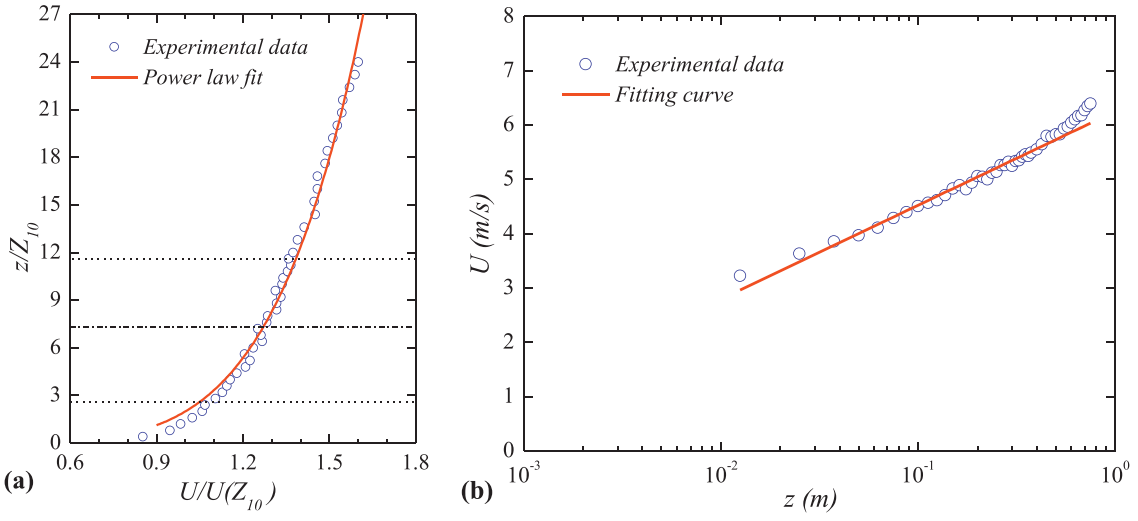

Fig. 2. Measured mean stream-wise velocity profile of the ABL wind. The figure (a) is in linear units, while the figure (b) is in linear-logarithmic units (In figure (a), horizontal dotted lines represent the top and bottom rotor tip heights, while the dash-dotted line indicates the turbine hub height).

represents the non-dimensional averaged wind velocity $U/U(Z_{10})$, where $U(Z_{10})$ is the velocity at a height of $Z_{10} = 31.25\ mm$ above the wind tunnel floor, which is equivalent of 10 m height above the ground in a full-scale wind farm with the scale ratio of 1:320. Fig. 2(a) clearly shows that the present measurement data can be fit well with the power law. According to ASCE standard (ASCE, 2005), the power law exponent for an ABL wind over natural open terrain usually ranges from 0.1 to 0.2. As shown in Fig. 2(a), the power law exponent of the curve fit to the present measurement data is 0.16, which is well within the range of ABL wind over open terrain.

In Fig. 2(b), the measured stream-wise velocity profile is fitted using a logarithmic profile. A friction velocity of $u_* = 0.3\ m/s$ is determined by using the measured Reynolds shear stress (see Fig. 3(b)). The fitted surface roughness length and zero plane displacement can then be obtained by fitting a logarithmic profile to the measured mean velocity. The fitted surface roughness length is approximately $z_0 = 0.24\ mm$. For the scaled ABL wind, this surface roughness length can translate into a roughness with an average height of approximately 8 *cm*, which is consistent with open terrain or grassland containing a small amount of scattered obstacles with heights approximately 1.5–10 *m*, as described in Australian Standard (AS/NZ1170.2, 2002). The fitted zero plane displacement is approximately $d = 0.16\ mm$. It should be noted that the experimental data in the near-wall region ($z \leq 38.1\ mm$) do not fit the logarithmic profile very well. In the present study, the turbine hub height is $H = 225\ mm$, which is much larger than the near-wall region mentioned above (i.e., $z \leq 38.1\ mm$). Our focus will be mainly on heights between $85\ mm \leq z \leq 365\ mm$ (i.e., heights corresponding to the rotor plane region of model wind turbine).

The turbulence intensity profiles for the simulated ABL flow are given in Fig. 3(a). The turbulence intensities are calculated as $I_u = \sigma_u/U_{local}$, $I_v = \sigma_v/U_{local}$ and $I_w = \sigma_w/U_{local}$, where σ_u, σ_v and σ_w are the root mean square of the velocity fluctuations in the stream-wise, span-wise and vertical directions, respectively. U_{local} is the time-averaged velocity at the measurement point. It can be seen that the turbulence intensities follow the relation $I_u > I_v > I_w$, which agree with the observations of Panofsky and Dutton (1984). In addition, as shown in Fig. 3(a), the stream-wise turbulence intensities (i.e., I_u) in the turbine rotor plane region are approximately 0.18. The standard stream-wise turbulence intensity profile of an ABL wind over an open terrain as suggested by Architectural Institute of Japan (AIJ, 1996), which is scaled at a ratio of 1:320, was also plotted in Fig. 3(a) for comparison. It can be clearly seen that the turbulent boundary layer flow generated inside the wind tunnel can be used to simulate the ABL wind over an open terrain in nature reasonably well. Fig. 3(b) shows the Reynolds shear stress profile of the simulated ABL flow normalized by the square of the friction velocity (i.e., u_*^2). The Reynolds shear stress increases with the height, reaches a peak at a short distance from the wall and then decreases with further increase in height. Similar trends of Reynolds shear stress were reported in the previous wind tunnel studies conducted by Chamorro and Porté-Agel (2009), Cal et al. (2010) and Markfort et al. (2012).

Fig. 3(c) gives the vertical profile of the stream-wise turbulence integral length scale (L_u^x), which is calculated using the direct integration of auto-correlation function based on the Taylor "Frozen Turbulence" hypothesis:

$$L_u^x = U\int_0^{\tau_{0.05}} R_u(\tau)\, d\tau \tag{1}$$

As indicated by Flay and Stevenson (1998), the error caused by Taylor "Frozen Turbulence" hypothesis would increase dramatically when the auto-correlation coefficient is very small. They suggested that the upper limit of the integral is taken $R_u(\tau) = 0.05$ as the best. Therefore, $\tau_{0.05}$ in Eq. (1) is the delay time corresponding to the auto-correlation coefficient $R_u(\tau)$ monotonically decreasing from 1 to 0.05. It should be noted that the turbulence integral length scale shown in Fig. 3(c) decreases continuously with increasing height, which differs from what is expected for ABL wind. This limitation can be traced to the structural characteristics of the triangular spires with narrow top and wide bottom. Still, it can be seen in Fig. 3(c) that the calculated L_u^x at turbine hub height is approximately 0.56 *m*, which could translate into a turbulence integral length scale of approximately 180 *m* for the full-scale ABL wind. This turbulence integral length scale (i.e., 180 *m*) is close to the empirical value as suggested by Counihan (1975) and Architectural Institute of Japan (AIJ, 1996).

The power spectrum, which reflects the distribution of the averaged power of fluctuating wind as a function of frequency, is an important characteristic of ABL wind. The Kaimal spectrum (Kaimal et al., 1972) is one of the most commonly used power spectra and can be expressed as:

$$\frac{nS_u(n)}{\sigma_u^2} = \frac{200\chi}{6(1+50\chi)^{5/3}} \tag{2}$$

where n is the frequency, $S_u(n)$ is the power spectral density and σ_u is the standard deviation of the fluctuating velocity at the measurement point. $\chi(= nz/U)$ is the reduced frequency, where U is the mean wind speed at height z.

Fig. 4 shows the power spectrum of the stream-wise velocity component measured at turbine hub height, which is calculated using a fast Fourier transform (FFT) analysis procedure with the multi-taper method (MTM). To improve the statistics of wavenumbers in the lower frequency range, 2^{16} bins are used for the FFT in the range of $\chi < 0.2$, while 2^{12} bins are used in the range of $\chi > 0.2$. It can be seen that the power spectrum profile of the measured velocity agrees reasonably with the Kaimal spectrum.

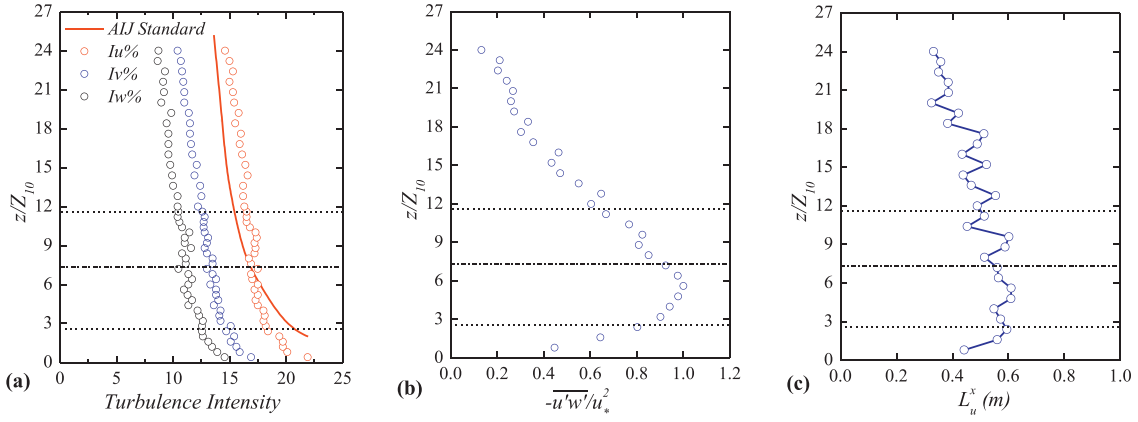

Fig. 3. Simulated ABL wind (a) Turbulence intensities and (b) Reynolds shear stresses (c) Stream-wise turbulence integral length scale.

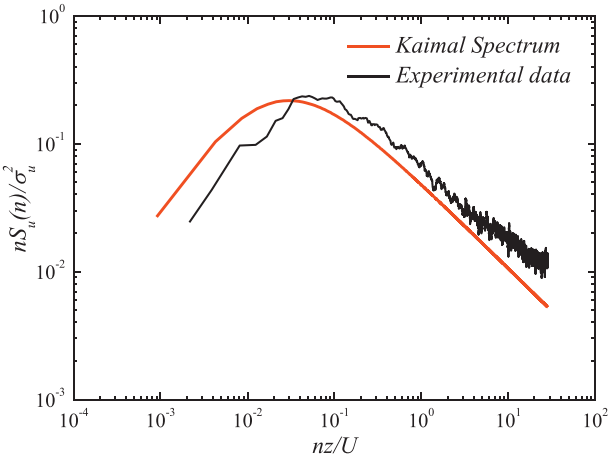

Fig. 4. Power spectrum of the stream-wise velocity component measured at turbine hub height.

2.2. The tested wind turbine and terrain models

The wind turbine model uses a scale ratio of 1:320, which is determined by the height ratio of the simulated ABL wind as mentioned above. The rotor radius of the wind turbine model is $R = 140$ *mm* and the turbine hub height is H=225 *mm*. Based on the ERS-100 prototype of the wind turbine blade developed by TPI Composites Inc., the blade model sections were generated by mathematically applying a spline under tension to interpolate between the defined input locations. As shown in Fig. 5, a circular section extending from the root of the blade to a distance of 5% of the blade radius (R) and three NREL airfoils (S819, S820, S821) placed at various locations were used as inputs to generate the blade profile. The S821 root airfoil was used between 0.208R and 0.40R; the S819 primary airfoil was positioned at 0.70R; and the S820 tip airfoil was specified at 0.95R. While the primary design parameters of the model turbine are listed in Table 2, further information about the ERS-100 rotor blades are available in Locke and Valencia (2004) and Somers (2005). Experiments using similar turbines include Tian et al. (2014) and Yuan et al. (2014).

In general, the Reynolds number of the large-scale wind turbine in atmospheric flow cannot be matched by wind-tunnel experiments. The Reynolds number based on the averaged chord length of the rotor blades (C) and the oncoming wind speed at the hub height (U_{Hub}) was found to be approximately 7000. This Reynolds number is significantly low compared to that of a large-scale wind turbine that is typically in the range of 0.7×10^6 to 10×10^6 (Wilson, 1994). However, as suggested by Medici and Alfredsson (2006), the behavior of the turbulent flow in the wake of a wind turbine would be nearly independent of the chord Reynolds numbers of the wind turbine. Furthermore, the main purpose of the present study was not to evaluate the performance of a full-scale wind turbine but to provide experimental data under well-controlled flow conditions for the validation of numerical simulations. As indicated by Adaramola and Krogstad (2011), Grant et al. (1997), Vermeer et al. (2003) and Haans et al. (2008), as a test case for numerical simulations, a lower Reynolds number is acceptable as long as the aerodynamic performances of the airfoils used for the model wind turbine are known. Therefore, the experimental data obtained in the present study can still be used if the numerical simulation is conducted at the model scale Reynolds number range.

Table 2
The primary design parameters of the wind turbine model.

Parameter	R	H	d_{rod}	$d_{nacelle}$	α	a	a1	a2
Dimension (mm)	140	225	18	26	5	68	20	35

In the present study, the rotational frequency of the turbine rotor was controlled by applying different electric loads to a small DC generator placed inside the turbine nacelle. The rotational speed of wind turbine Ω can change from 0 to 2 200 rpm, which corresponds to the tip-speed-ratio (i.e., $\lambda = \Omega R/U_{Hub}$) changing from 0 to 6.5. For each tested case, a series of tip-speed-ratio values were adjusted to search for the optimum tip-speed-ratio (i.e., the tip-speed-ratio with maximum power output of the model wind turbine). All the dynamic load data presented in this study were obtained with the model turbine operating under the optimum tip-speed-ratio.

As shown in Fig. 6, two typical two-dimensional hill models with different slopes were made of wooden frames and thin film covers. The geometry of the two-dimensional hill model with a Gaussian curve is defined by the following relationship:

$$Z = h*\exp\left[-\left(\frac{x}{L}\right)^2 \ln 2\right] \tag{3}$$

where $h = 285$ *mm* is the height of the hill model, and L is the length measured in the flow direction between hill height form $h/2$ to h. The hill slope is defined as $s=(h/2)/L$. As shown in Fig. 6, the two hill models with slope of $s = 0.25$ (i.e., gentle hill) and $s = 0.5$ (i.e., steep hill) were tested in the present study. According to the study of Mason and King (1985), the critical slope for the occurrence of flow separation over hilly terrain is approximately 0.3. Therefore, the two hill models shown in Fig. 6 can be used to represent typical hilly terrains with and without

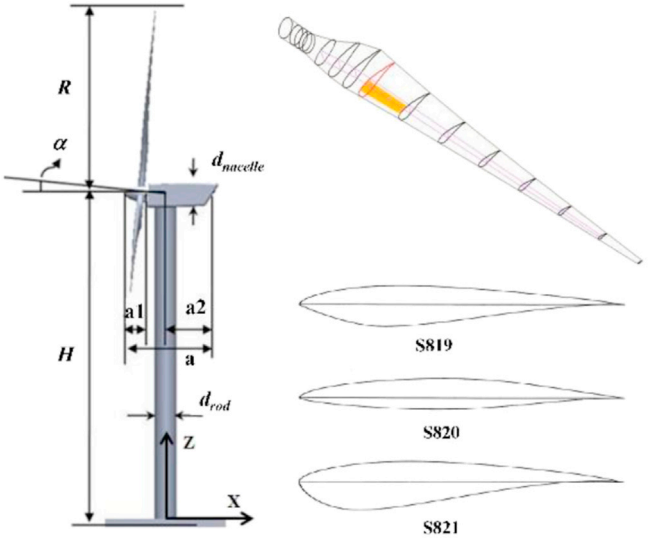

Fig. 5. Schematic diagram of the wind turbine model.

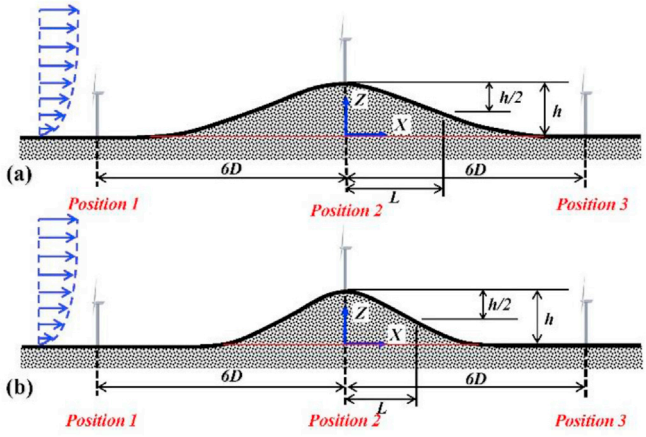

Fig. 6. Schematic diagram of the hill models (a) Gentle hill; (b) Steep hill.

flow separation on the lee side.

In addition, as shown in Fig. 6, three typical positions, which are located 6*D* in front of the hilltop, on the hilltop and 6*D* behind the hilltop, were chosen to investigate the terrain effects on the performance of the wind turbine sited on the hill model, where D=280 *mm* is the diameter of the turbine rotor. First, the dynamic wind loads of a single wind turbine installed on the hilltop and 6*D* behind the hilltop were tested. Second, after installing three wind turbine models at the selected positions, the dynamic wind loads of the downstream wind turbines sited on the hilltop and 6*D* behind the hilltop were measured. Third, flow measurements were conducted on the hilltop and 6*D* behind the hilltop to reveal the effect of topography on the evolution of the upstream turbine wake. During the experiments, in order to measure the wake characteristics at the selected position, the wind turbine model was removed before the flow measurements were conducted at that position. Furthermore, experiments with three wind turbine models aligned in the free-stream direction with *6D* spacing on flat surface were also conducted for comparison.

It should be noted that the blockage of the wind tunnel cross section caused by the hill model was approximately 12.5%. This is higher than the suggested upper limit of the blockage effect to avoid wind tunnel wall effects on the measurements. The blockage effect should be considered when the data are studied. However, as suggested by Røkenes and Krogstad (2009), because the main objective of the present study was to obtain data for the validation and verification of the numerical simulations, the blocking effect may be accounted for in the calculations by setting the computational boundaries at the wind tunnel walls.

2.3. Dynamic wind loads and flow field measurements

In the present study, a high-sensitivity load cell (JR3, model 30E12A-I40) was used to measure the dynamic wind loads acting on the wind turbine model. The JR3 load cell was mounted at the tower base of the wind turbine model, and it can provide instantaneous measurements of the aerodynamic forces and moment (torque) about all three axes. The measurement range of the JR3 load cell is 40 *N* for aerodynamic forces and 5 $N \bullet m$ for moment (torque). While similar wind loads features were revealed by different components of the aerodynamic forces and the moments, only the measured thrust coefficient, C_T, is given in the present study for conciseness. The coefficients of the thrust force were calculated by using following equation:

$$C_T = \frac{T}{\frac{1}{2}\rho U^2 \pi R^2} \tag{4}$$

where ρ is the air density. During the experiments, the sampling rate of the wind load data was 1000 Hz. For each test case, the sampling time was set to be 60 s to ensure sufficient convergence of the mean and standard deviation of the measured thrust force. In addition, according to the sampling theorem, the analyzable frequency for the measured thrust force is in the range of 1/120 Hz–500 Hz with the frequency resolution of 1/60 Hz.

A Cobra Probe anemometry system was applied to measure the turbulent flow over the hill, as well as the flow in the wake behind the wind turbine model. By using this Cobra Probe, all three components of velocity vector could be measured instantaneously. During the experiments, the maximum flow velocity measured in the wind tunnel is approximately 8 m/s. The relative uncertainty of the Cobra Probe anemometry is 1.50% for 8 m/s which is 0.12 m/s. The accuracies of all the other velocity values measured in the present study are within ± 0.12 m/s. The sampling rate of the instantaneous velocity vector was 1250 Hz with a measurement period of 60 s at each point of interest. The selected sampling time (i.e., 60 s) ensure sufficient convergence for the higher-order statistical analysis of the components of the measured velocity vector, such as the turbulence intensity, turbulence kinetic energy and Reynolds shear stress. Based on the selected sampling rate and sampling time, the analyzable signal frequency range for the measured velocity vector is 1/120 Hz–625 Hz with the frequency resolution of 1/60 Hz.

To interpret the terrain effect more clearly, the stream-wise mean velocity measured in the oncoming ABL wind profile over a flat surface at the turbine hub height (i.e., U_{Hub}) is used as the reference velocity in Section 3. During the experiments, the reference velocity was held constant at U_{Hub}=5.0 m/s. In addition, while the height from the local surface in the hill model is denoted by z, Z is used to represent the height from the wind tunnel floor.

3. Results and discussion

3.1. Flow characteristics over hilly terrain with different slopes

Five positions (i.e., $x/D = -6,\ -3,\ 0,\ 3,\ 6$, and $x = 0$ corresponds to the stream-wise location of the hilltop) were selected to measure the turbulent flow characteristics over the tested hill models. The comparison of stream-wise velocity profiles between the gentle and steep hill models are plotted in Fig. 7. The stream-wise mean velocity profile of the oncoming ABL wind on the flat surface was also plotted for comparison. As expected, no flow separation can be observed for the gentle hill, while flow separation occurs for the steep hill.

The fractional speed-up ratio, which is defined as $\Delta S = (U(z) - U_0(z))/U_0(z)$, is usually used to quantify the speed-up effect over a hilly terrain, where $U_0(z)$ is the mean velocity of the oncoming ABL flow on a flat surface. The fractional speed-up ratio profiles obtained at different locations over the gentle and steep hill models are plotted in Figs. 8 and 9, respectively. The results reported by Kim et al. (1997), Gong and Ibbetson (1989) and Cao and Tamura (2006) with similar hill slopes and test conditions as those of the present study are given for quantitative comparison. In addition, the standard profiles suggested by wind loading codes (ASCE, 2002; AS/NZ1170.2, 2002; CEN, 2004) were also plotted in the figures for comparison.

For the gentle hill, it can be seen that the measurement results are in good agreement with the profiles provided by wind loading codes except for the near-wall region. At the location of $x = -3D$, the discrepancies in the near-wall region indicate that the wind loading codes cannot accurately reveal the blocking effect caused by the downstream hill. At the locations of $x = 3D$ and $x = 6D$, the distinct velocity deficits caused by the high adverse pressure gradient in the near-wall region also cannot be revealed correctly by the wind loading codes. As comparison with the previous studies, it can be seen in Fig. 8(b) and (c) that the speed-up ratios at $x = -3D$ and $x = 0$ were slightly lower than those reported by Kim et al. (1997) and Gong and Ibbetson (1989). In addition, at the locations of $x = 3D$ and $x = 6D$, the velocity deficits in the near-wall region were also lower than the results provided by Kim et al. (1997) and Gong and Ibbetson (1989). These discrepancies are believed to be attributed to the different hill slopes (i.e., $s = 0.25$ for the present study vs. $s = 0.30$ for Kim et al. (1997) and $s = 0.31$ for Gong and Ibbetson (1989)).

For the steep hill, it can be seen in Fig. 9 that the measurement data are in good agreement with the experimental results provided by Kim et al. (1997) and Cao and Tamura (2006). As comparison with the wind loading codes, the discrepancies in the near-wall region shown in Fig. 9(b) also indicate that the wind loading codes cannot accurately reveal the blocking effect caused by the downstream hill. In addition, as shown in Fig. 9(d), the results obtained at the location of $x = 3D$ show significant difference when compared with the profiles provided by the wind loading codes. This difference could be attributed to the fact that the data suggested by the wind loading codes are mainly derived using linear theory, which has very poor ability to predict the flow characteristics in the separation region on the lee side of a steep hill.

While the mean wind speed distributions over the hilly terrains are closely related to the amount of power that can be extracted by the wind turbines, the turbulence levels of the flows are directly associated with the fatigue loads acting on the wind turbines. Because the flow direction

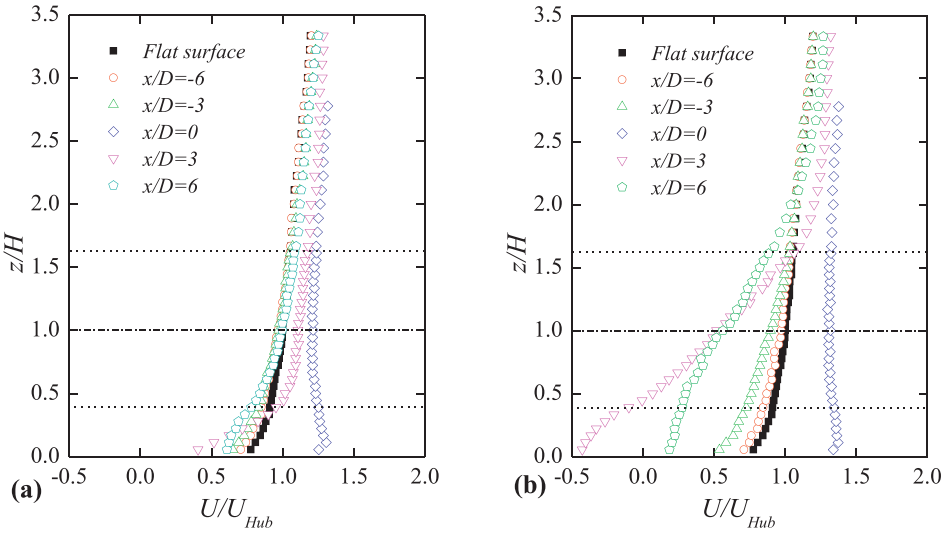

Fig. 7. Comparison of stream-wise mean velocity profiles at different locations (a) Gentle hill, (b) Steep hill.

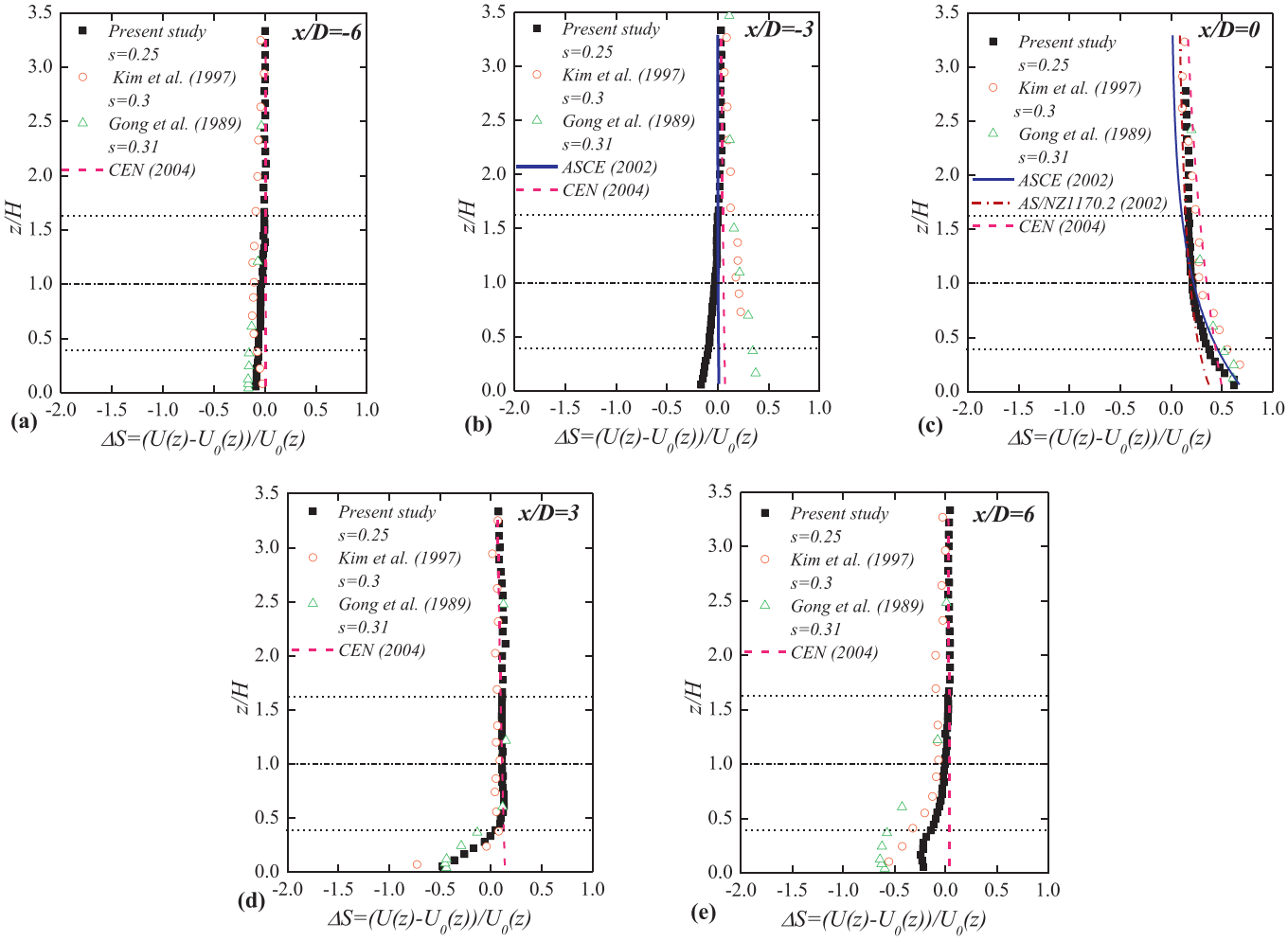

Fig. 8. The fractional speed-up ratio profiles measured at different locations over the gentle hill (a) $x = -6D$, (b) $x = -3D$, (c) $x = 0$, (d) $x = 3D$ and (e) $x = 6D$.

changes significantly over hilly terrain, the turbulence kinetic energy (TKE), which is calculated by summing the fluctuation of velocity in three directions, is used in the present study to analyze the turbulent characteristics. The TKE is calculated by using the following equation:

$$TKE = \frac{\frac{1}{2}\left(\sigma_u^2 + \sigma_v^2 + \sigma_w^2\right)}{U_{Hub}^2} \tag{5}$$

where σ_u, σ_v, σ_w are the standard deviations of the fluctuating velocities

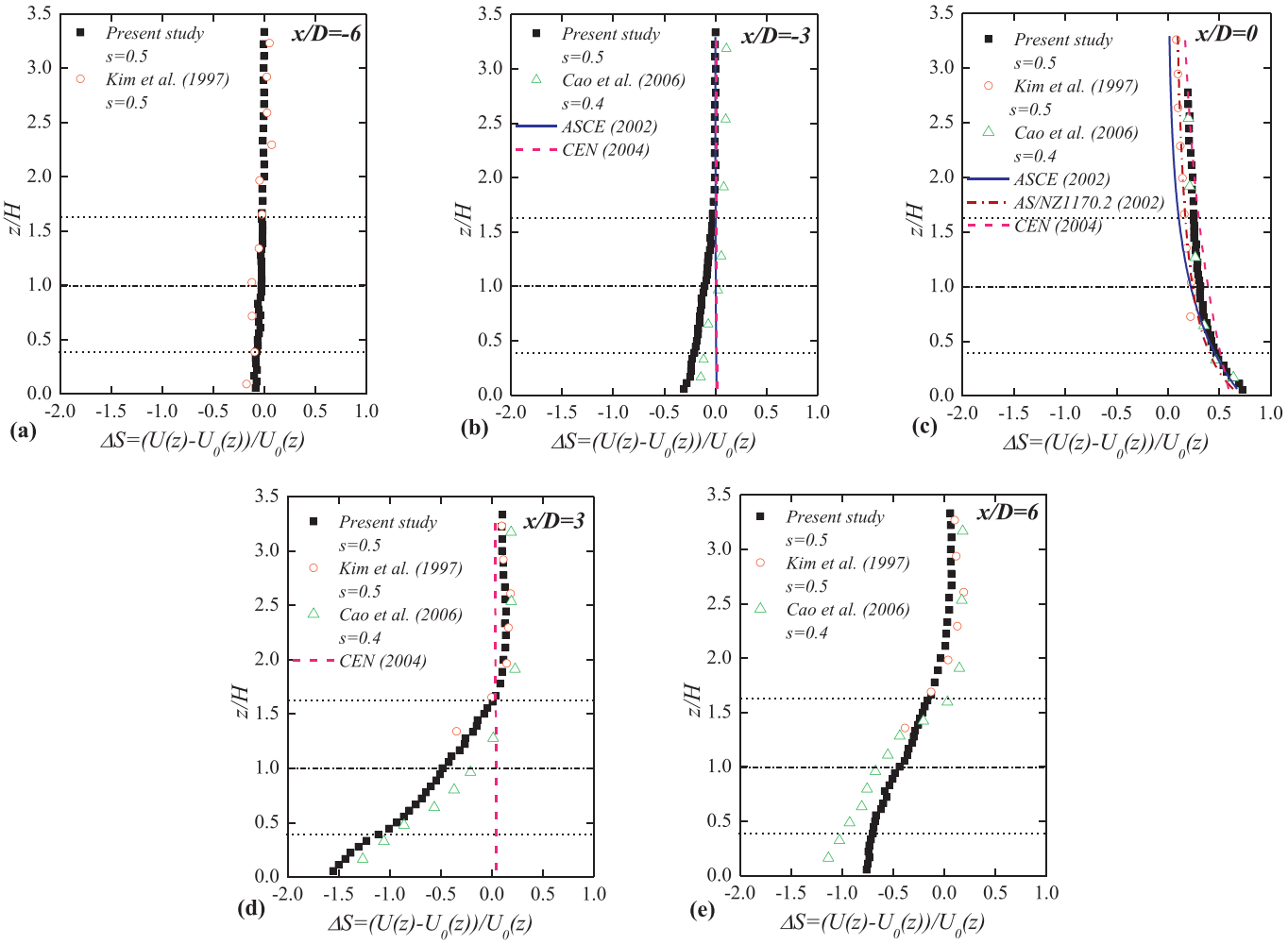

Fig. 9. The fractional speed-up ratio profiles measured at different locations over the steep hill (a) $x = -6D$, (b) $x = -3D$, (c) $x = 0$, (d) $x = 3D$ and (e) $x = 6D$.

in stream-wise, span-wise and vertical directions, respectively.

The TKE profiles for both the gentle and steep hill models are plotted in Fig. 10. The TKE profile of the oncoming ABL wind on the flat surface was also plotted for comparison. While no appropriate TKE data can be found in previous studies to compare with that of the steep hill, the results reported by Kim et al. (1997) with hill slope of $s = 0.3$ were plotted in Fig. 10 to compare with the TKE profiles over the gentle hill. It can be seen that for the gentle hill, the measurement results of the present study are in good agreement with the results reported by Kim et al. (1997). For the gentle hill, the change of the TKE distributions appears mainly at the locations behind the hilltop. With flow moving over the downgrade of the hill, the increase of TKE mainly occurred in the region below the hill height. However, compared to the gentle hill, the variations of the TKE distributions at the locations behind the steep hill are much more significant due to the flow separation. As shown in Fig. 10(d) and (e), the expansion of the regions with high TKE is extremely large for the steep hill case. At the location of $x = 6D$, the flow with high TKE levels can expand to the height of $z/H = 3.0$, which is two times higher than the hill height.

In addition, as shown in Fig. 10(c), for both the gentle and steep hills, the TKE values measured on the hilltops are slightly lower than those of the oncoming ABL wind on the flat surface. It can be concluded that the hill will have a positive effect on a wind turbine sited on a hilltop for virtually any hill slopes, not only by increasing the flow velocity due to the speed-up effect but also by decreasing the turbulence level of the flow on the hilltops.

3.2. Wind turbine sited on top of the hills

3.2.1. Dynamic wind loads acting on single wind turbines sited on the hilltops

As mentioned above, a JR3 load cell was used to measure the thrust force acting on the wind turbine model. In the present study, the maximum thrust force acting on the wind turbine model is approximately 1.0 *N*. The uncertainty of the JR3 load cell is approximately 0.02 *N* for 1.0 *N*. The accuracies of all the other thrust forces measured in the present study are within ±0.02 *N*.

In the present study, the thrust coefficients are defined using two different approaches. First, the thrust coefficients were calculated by using a constant reference velocity (i.e., U_{Hub}=5.0 m/s, which is the oncoming ABL wind velocity at hub height of the wind turbine sited on the flat surface). The means and standard deviations of the thrust coefficients calculated by using U_{Hub}=5.0 m/s as reference velocity are listed in the first and second lines of Table 3. The thrust coefficient of the turbine model mounted on the flat surface is also listed for comparison. As expected, the high flow velocity caused by the speed-up effect leads to a significant increase in the mean wind loads acting on the wind turbine model. Compared to the case of flat surface, the increased thrust forces acting on the wind turbines sited on top of the gentle and steep hills reach 33% and 47%, respectively. According to the momentum and energy conservation laws, while the aerodynamic thrust force acting on a wind turbine is proportional to the momentum deficits in the square of the flow velocity across the rotation disk of the wind turbine, the power output of the wind turbine (i.e., the wind energy harvested by the wind turbine) would be proportional to the deficits in the cube of the flow velocity (i.e.,

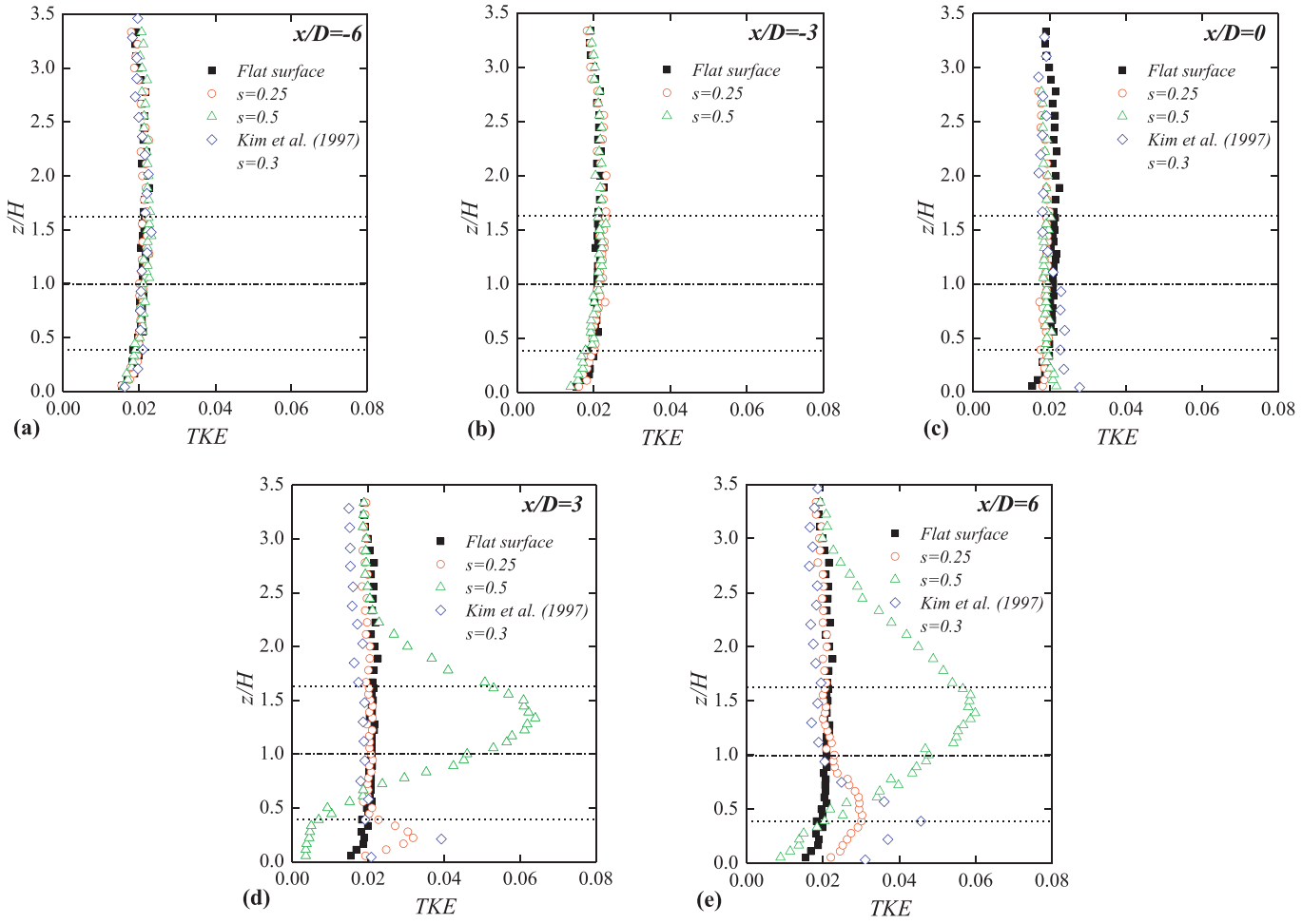

Fig. 10. Comparison of TKE profiles at different locations over the gentle and steep hills (a) $x = -6D$, (b) $x = -3D$, (c) $x = 0$, (d) $x = 3D$ and (e) $x = 6D$.

Table 3
Dynamic thrust coefficients acting on single wind turbine sited on the hilltops and the flat surface.

Wind load measurement results	Gentle hill	Steep hill	Flat surface
Mean thrust coefficient (U_{Hub}=5 m/s as reference velocity)	0.68	0.75	0.51
Standard deviation of the thrust coefficient (U_{Hub}=5 m/s as reference velocity)	0.21	0.20	0.23
Local hub height velocity, $U_{Hub,\ local}$ (m/s)	6.0	6.6	5.0
Mean thrust coefficient ($U_{Hub,\ local}$ as reference velocity)	0.47	0.43	0.51
Standard deviation of the thrust coefficient ($U_{Hub,\ local}$ as reference velocity)	0.15	0.11	0.23

the differences in flow kinetic energy) across the rotation disk. With the turbine model mounted on the hilltops, the higher mean wind loads are believed to be closely related to the improved wind energy harnessing. In addition, while the mean thrust forces acting on the wind turbines sited on the hilltops are much higher than that of the flat surface, the standard deviations of the dynamic wind loads acting on the wind turbine sited on the hilltops are slightly lower than that of the flat surface case. This slight decrease is in accordance with the TKE distributions on the hilltops, as shown in Fig. 10(c).

Second, the thrust coefficients were calculated by using the local hub height velocity (i.e., $U_{Hub,\ local}$, which is the hub height velocity measured at the location where the tested wind turbine will be mounted). The results are listed in the fourth and fifth lines of Table 3. Interestingly, it can be seen that both the means and standard deviations of the thrust coefficients acting on the wind turbines sited on the hilltops were smaller than that of the flat surface case, especially for the standard deviations of the thrust coefficients. It can be deduced that, for the same hub height velocity, the decrease of means and standard deviations of the wind loads acting on the wind turbines sited on the hilltops would become more pronounced with the increase of hill slope.

As shown in Fig. 11, the histograms of the measured thrust coefficients acting on the wind turbine models sited on the hilltops were fitted quite well by a Gaussian function. The study of Hu et al. (2012) indicated that the histogram of dynamic wind loads acting on the wind turbine experiencing ABL wind could be reasonably fitted with a Gaussian distribution, which can also be observed in the present study, as shown in Fig. 11(c). Compared to the flat surface, the closer matches between the measurement results and the Gaussian distributions for the wind turbines sited on the hilltops are believed to be closely related to more uniform flows with lower turbulence levels experienced by the wind turbines. The good agreement with a Gaussian distribution confirms that the standard deviations of the dynamic wind loads listed in Table 3 can be used as a quantitative parameter to evaluate the fatigue loads acting on wind turbines sited on the hilltops.

Fig. 12 shows the power spectra of the measured fluctuating thrust coefficients obtained using an FFT analysis procedure, which reveals the amplitudes of the fluctuating thrust coefficient at different frequencies. In order to evaluate the turbulent flow over complex terrains, the ABL wind simulated in the present study was controlled at a relatively high turbulence level. As shown in Fig. 3(a), the stream-wise turbulence intensities of the simulated ABL wind in the turbine rotor plane region can

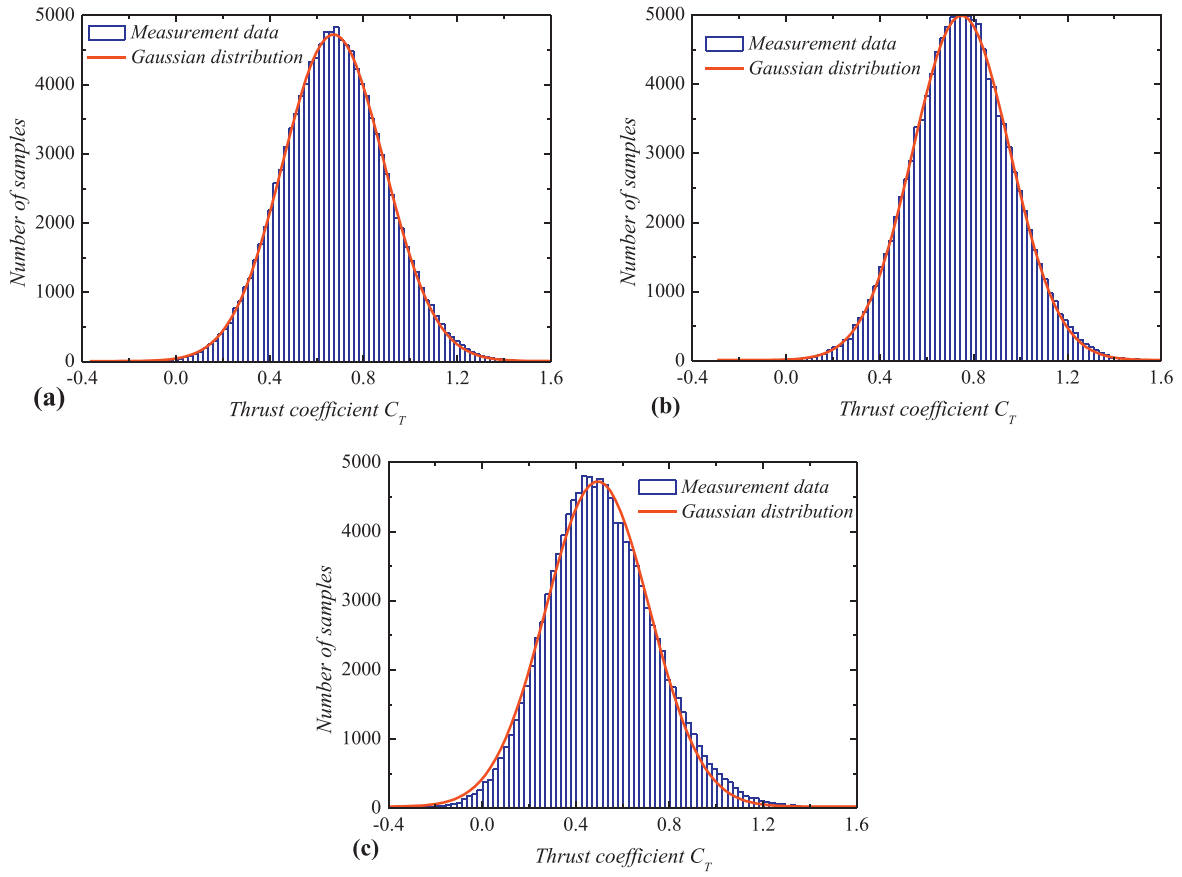

Fig. 11. Histograms of the instantaneous thrust force coefficients. (a) Single turbine sited on top of the gentle hill (b) Single turbine sited on top of the steep hill (c) Single turbine sited on the flat surface.

reach approximately 0.18. The behavior of dynamic wind loads acting on wind turbines under different types of ABL winds has been revealed by the study of Tian et al. (2014), which indicated that high turbulence in ABL flow would cause the rotational speed of the wind turbine to fluctuate in a wide frequency range, and no well-defined peak can be identified in the corresponding power spectrum. As shown in Fig. 10, there is no significant difference between the turbulence characteristics on the hilltops and the flat surface. Therefore, the power spectra of the measured dynamic wind loads shown in Fig. 12 have similar behavior. During measurement of the thrust force, a tachometer was used to simultaneously measure the instantaneous rotational speed of the wind turbine blades. The measurement data obtained by the tachometer also indicate that the inflow turbulence significantly affects the rotational speed of wind turbine blades. The behaviors of rotational frequencies revealed by the FFT analysis of the wind load measurements were found to agree well with the rotational speed of the rotor blades measured using the tachometer.

3.2.2. *Effect of the upstream turbine wake on the wind turbine sited on the hilltops*

Figs. 13 and 14 show the stream-wise mean velocity and TKE distributions measured on the hilltops with and without a model wind turbine mounted 6*D* in front of the hilltop. The flow characteristics measured 6*D* downstream of a model turbine sited on a flat surface are also plotted for comparison. As expected, due to the increase of the surface height, the wake of the upstream turbine mainly affected the flow near the surface of the hilltop. Only a slight velocity deficit and enhanced TKE can be observed in the region of the rotation disk of the wind turbine sited on the hilltops. The effect of hill slope on the evolution of the turbine wake can be also observed in Fig. 13. The velocity deficit reaches the height of $z/H = 0.6$ for the gentle hill, which is higher than that of the steep hill (i.e., $z/H = 0.5$). Therefore, compared to the steep hill, the upstream turbine wake could expand into a wider region as it traveled up the hill with gentle slope.

The dynamic wind loads measured at the tower base of the wind turbines sited on the hilltops with and without the wake interference of the upstream turbine are shown in Table 4. The data from a wind turbine located 6*D* behind an upstream turbine on the flat surface are also listed for comparison. Compared to the flat surface case, the effects of the upstream turbine wake on the thrust forces are much less distinct for the wind turbines sited on the hilltops. The decreases of mean thrust forces caused by the velocity deficit are only approximately 4.4% and 2.6% for the gentle and steep hills, respectively, which are much lower than that of the flat surface case (i.e., 12%). As described above, the standard deviations of the dynamic wind loads represent the fluctuations that could be correlated to the fatigue loads acting on the wind turbine. As listed in Table 4, the effects of the upstream turbine wake on the fatigue loads acting on the downstream turbine models sited on the hilltops were found to be rather small (i.e., within the range of the measurement uncertainty), which agrees reasonably well with the TKE distributions shown in Fig. 14.

3.3. *Wind turbine sited behind the hills*

3.3.1. *Dynamic wind loads acting on a single wind turbine sited behind the hills*

The means and standard deviations of the thrust coefficients acting on the wind turbines mounted 6*D* behind the top of the gentle and steep hills (calculated by using U_{Hub}=5.0 m/s as reference velocity) are listed in the first and second lines of Table 5. As described in Section 3.1, the flow characteristics behind the gentle and steep hills show significant differences due to the flow separation. As expected, due to the distinct velocity

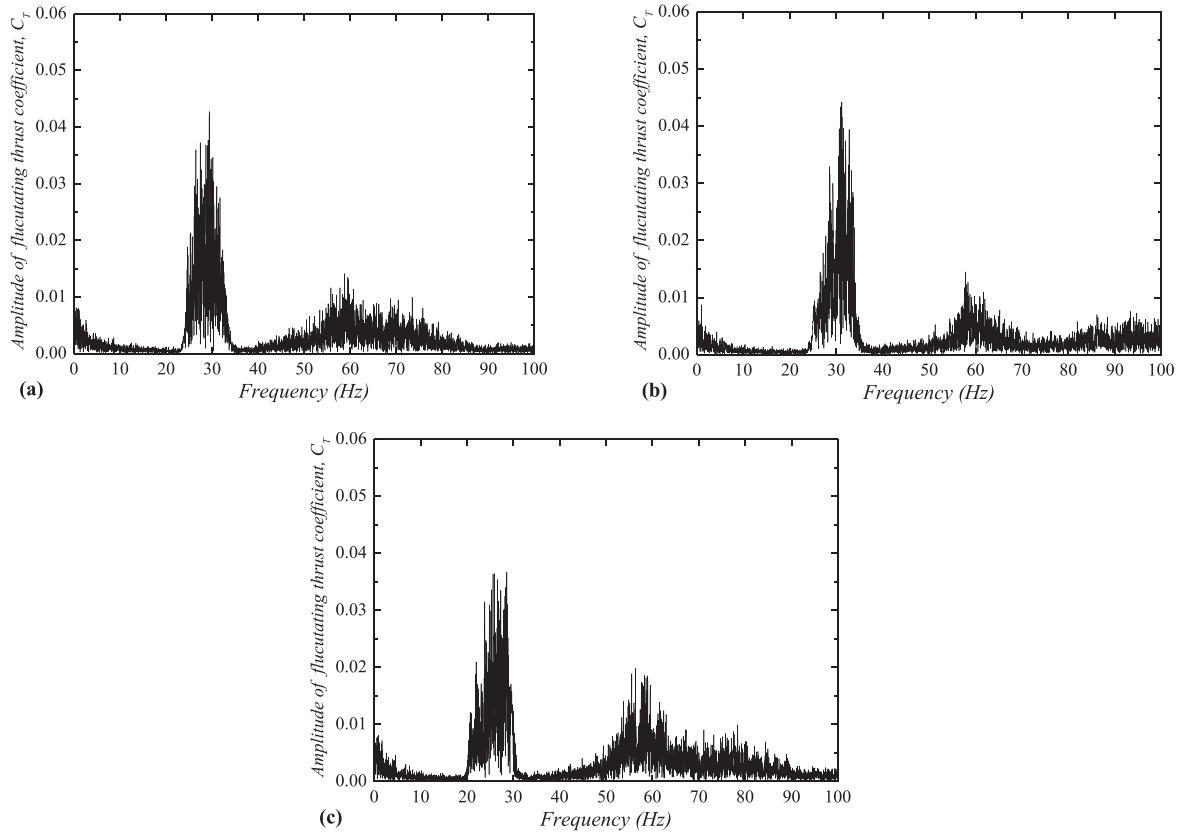

Fig. 12. Power spectra of the instantaneous thrust forces. (a) Single turbine sited on top of the gentle hill (b) Single turbine sited on top of the steep hill (c) Single turbine sited on the flat surface.

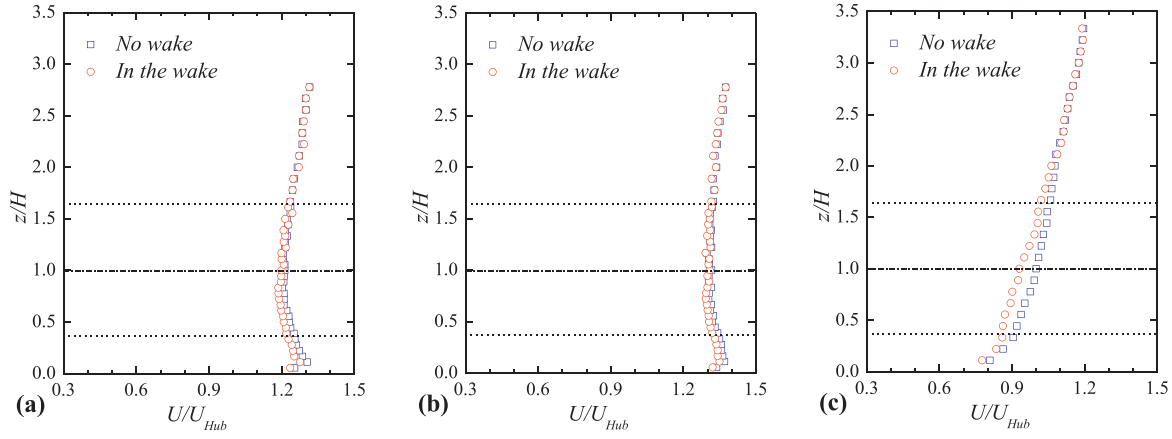

Fig. 13. Comparison of velocity profiles with and without the effect of the upstream turbine wake. (a) Measured on top of the gentle hill (b) Measured on top of the steep hill (c) Measured on the flat surface.

deficit caused by the terrain effect, the thrust force acting on the wind turbine sited 6*D* behind the top of the steep hill decreases significantly to only approximately 31% of that of a single wind turbine sited on the flat surface. For the gentle hill, as shown in Fig. 7(a), the topographic effect at the location 6*D* behind the hilltop is relatively small, and the velocity deficit mainly occurs in the near-wall region. The mean thrust force acting on the wind turbine sited 6*D* behind the top of the gentle hill is 0.46, which is approximately 90% of that of a single wind turbine sited on the flat surface. In addition, while the mean thrust forces were found to correlate well with the characteristics of the mean flow velocity profiles, the variations in the standard deviations of the thrust forces were closely related to the measured TKE profiles. Due to the enhanced TKE shown in Fig. 10(e), the standard deviation of the thrust force for the gentle hill case was found to be 0.28, which is approximately 22% more than that of a single turbine sited on the flat surface.

In addition, the means and standard deviations of the thrust coefficients calculated by using local hub height velocity (i.e., $U_{Hub,\ local}$) are listed in the fourth and fifth lines of Table 5. A key point here is that for the same hub height velocity, the standard deviation of the thrust coefficient acting on the wind turbine sited behind the steep hill is much higher than that of a single wind turbine sited on the flat surface. This dramatic increase of standard deviation of the thrust coefficient significantly shortens the lifetime of wind turbine sited behind the steep hill.

Fig. 15 shows the histograms of the measured thrust coefficients

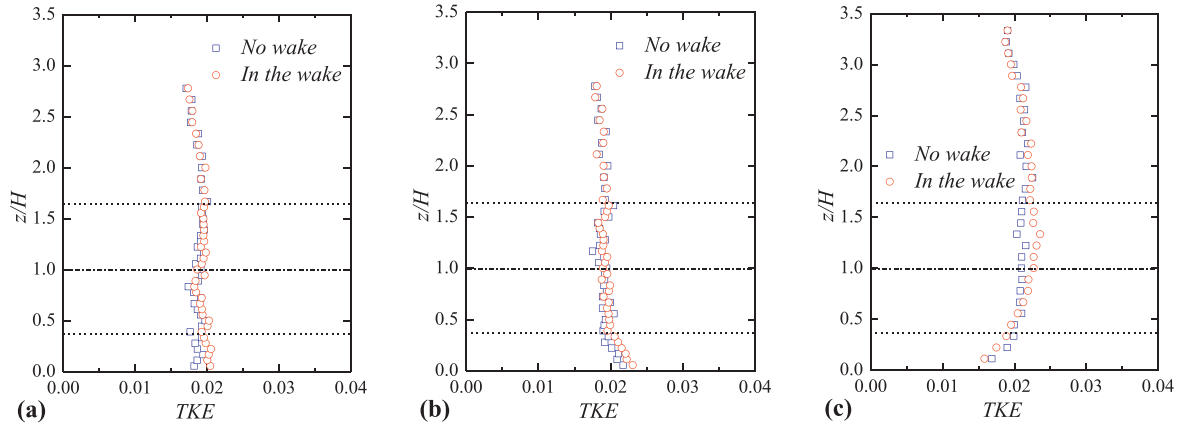

Fig. 14. Comparison of TKE profiles with and without the effect of the upstream turbine wake. (a) Measured on top of the gentle hill (b) Measured on top of the steep hill (c) Measured on the flat surface.

Table 4
Effect of upstream turbine wake on dynamic wind loads of downstream wind turbines sited on the hilltops (Using $U_{Hub} = 5$ *m/s* as reference velocity).

Wind load measurement results	Gentle hill		Steep hill		Flat surface	
	No wake	In the wake	No wake	In the wake	No wake	In the wake
Mean thrust coefficient	0.68	0.65	0.75	0.73	0.51	0.45
Standard deviation of the thrust coefficient	0.21	0.22	0.20	0.21	0.22	0.25

Table 5
Dynamic thrust coefficients acting on a single wind turbine sited 6*D* behind the hilltop.

Wind load measurement results	Gentle hill	Steep hill	Flat surface
Mean thrust coefficient (U_{Hub}=5 *m/s as reference velocity*)	0.46	0.16	0.51
Standard deviation of the thrust coefficient (U_{Hub}=5 *m/s as reference velocity*)	0.28	0.15	0.23
Local hub height velocity, $U_{Hub,\ local}$ *(m/s)*	5.0	2.8	5.0
Mean thrust coefficient ($U_{Hub,\ local}$ *as reference velocity*)	0.46	0.51	0.51
Standard deviation of the thrust coefficient ($U_{Hub,\ local}$ *as reference velocity*)	0.28	0.48	0.23

acting on the wind turbine models sited 6*D* behind the hilltops. For the gentle hill, the histogram of dynamic wind loads also can be reasonably fitted with a Gaussian distribution. However, compared to the flat surface and gentle hill cases, the wind turbine located behind the steep hill has a greater probability of experiencing extreme wind loads. The histogram shown in Fig. 15(b) indicates that the standard deviation of the dynamic wind loads would undervalue the fatigue loads acting on the wind turbine sited behind the steep hill, thereby overestimating the lifetime of the wind turbine.

The behavior of dynamic wind loads acting on the wind turbine is highly related to the local flow characteristics. The histograms of the instantaneous hub height velocity measured 6*D* behind the top of the gentle and steep hills (i.e., the locations where the wind turbine models will be mounted) are plotted in Fig. 16. The histogram of the hub height velocity measured on the flat surface is also plotted for comparison. It should be noted that Cobra Probe cannot measure the velocities in the opposite direction of the probe. Therefore, for the steep hill case, no negative velocities are being recorded at the measurement point, which cause the histogram distribution shown in Fig. 16(b) to rise sharply from zero. As shown in Fig. 16, the histogram distribution for the steep hill case shows a significant difference when compared with the gentle hill and the flat surface cases. The wind turbine sited behind the steep hill has a much higher chance of experiencing instantaneous wind speeds far from the mean value, which could be the reason for the greater probability of extreme wind loads acting on the wind turbine located behind the steep hill.

Fig. 17 shows the power spectra of the measured instantaneous thrust coefficients. The power spectrum corresponding to the steep hill is quite different from those of the flat surface and gentle hill cases. It can be seen form Fig. 17(b) that the rotational speed of the wind turbine sited behind the steep hill fluctuates in a wide range (i.e., from a frequency close to zero to a quite high frequency). It is difficult to distinguish the dominant frequency from the spectrum shown in Fig. 17(b). This behavior of rotation frequency agrees well with the rotational speeds of the rotor blades measured by using the tachometer. During the experiments, it can be observed that the rotational speeds of the wind turbine sited behind the steep hill fluctuated randomly over a wide range with its lower bound close to zero.

3.3.2. *Effect of upstream turbine wake on the wind turbine sited behind the hills*

After mounting a model turbine on the hilltops, the characteristics of the inflow experienced by the wind turbines sited 6*D* behind the hilltops were measured and are plotted in Figs. 18 and 19. For the gentle hill, with the expanding of the upstream turbine wake over the downgrade of the hill, the velocity deficit can be observed clearly at the location 6*D* behind the hilltop, and this velocity deficit is even higher than that of the flat surface, as observed by comparing Fig. 18(a) and Fig. 13(c). This increased velocity deficit indicates that the wake effect can be enhanced by the topography with flow moving downgrade of the gentle hill. This enhanced wake effect for the gentle hill could be attributed to the adverse pressure gradient over the downgrade of the hill, which restricts the turbulent mixing of the low-speed wake flow with the outer high-speed flow, thereby reducing the recovery of the wake flow.

Interestingly, Fig. 19(a) shows that the upstream turbine leads to a reduction in the TKE below the hill height (compared to the relatively high turbulence levels near the hill surface). This can be explained by the enhanced turbulent mixing in the turbine wake flow resulting in a weaker shear layer in the region below the hill height, as shown in Fig. 18(a), which would reduce the production of the TKE in this region. In the region above the hill height, the enhancement of TKE caused by the upstream turbine wake can be clearly observed in Fig. 19(a).

While the effect of the upstream turbine wake can be enhanced over the downgrade of the gentle hill, the wake of the wind turbine sited on the hilltop shows quite a different behavior as it moves over the downgrade of the steep hill. As described in Fig. 7(b), the hill with steep slope induces a flow separation behind the hilltop. The wind turbine sited 6*D*

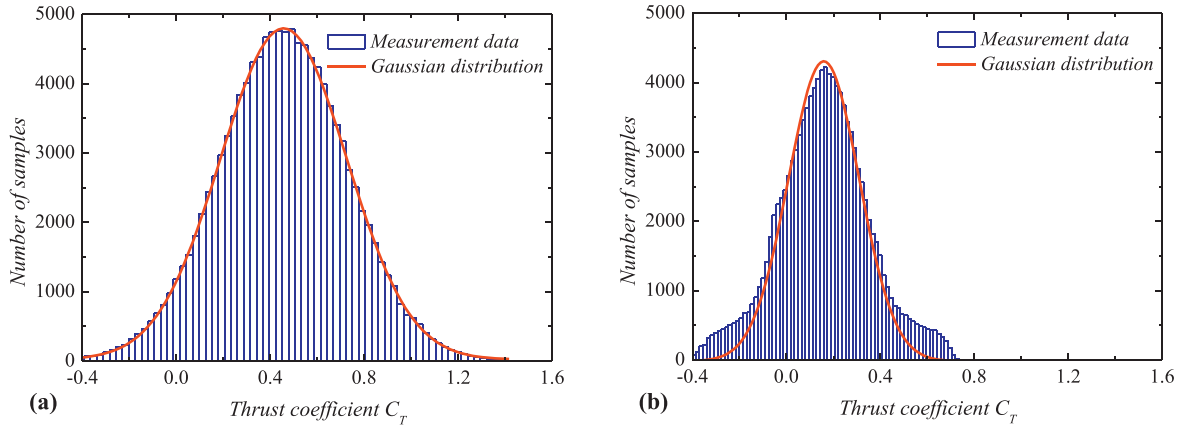

Fig. 15. Histograms of the instantaneous thrust coefficients. (a) Single turbine sited 6*D* behind the top of the gentle hill (b) Single turbine sited 6*D* behind the top of the steep hill.

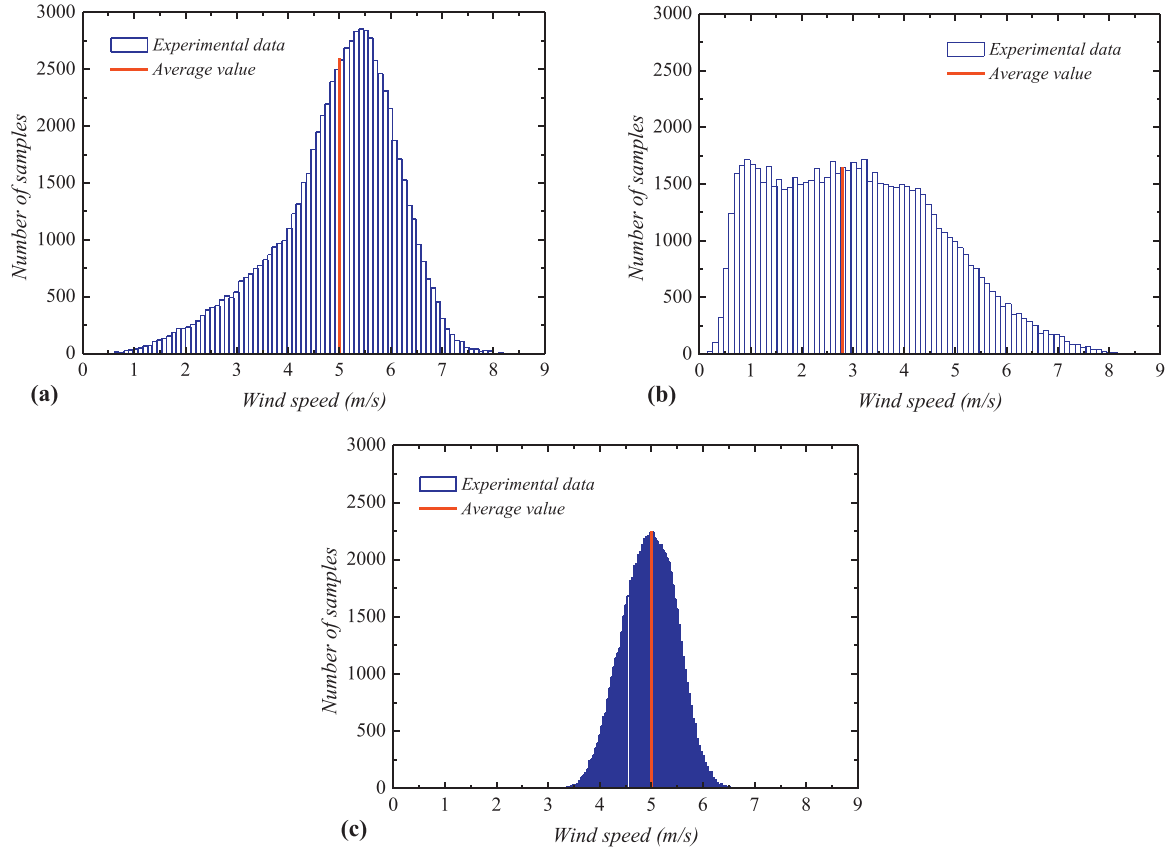

Fig. 16. Histograms of the instantaneous inflow wind speed measured at the local hub height. (a) 6*D* behind the top of the gentle hill (b) 6*D* behind the top of the steep hill (c) On flat surface.

behind the hilltop is immersed in the separated flow region. Compared to the significant change of flow velocity and TKE caused by the separated flow, the influence of the upstream turbine wake is negligibly small. Figs. 18(b) and 19(b) show that the measured velocity and TKE profiles are nearly independent of whether or not the upstream wind turbine is mounted on the hilltop.

Fig. 20 shows the comparison of the spectra of the flow velocities measured at the selected point $x = 6D$, $(z\text{-}H)/D = 0.5$ (i.e., top tip height of rotor blades of the wind turbines sited 6*D* behind the hilltops) with and without the upstream wind turbine mounted on the hilltop. The spectra shown in Fig. 20 are normalized by U_{Hub}, H and σ_u^2, whilst the horizontal axis represents the non-dimensional frequency nH/U_{Hub}. For the gentle hill, the spectrum of the stream-wise velocity in the wake of the upstream turbine presents an evident increase of the kinetic energy in the high frequency range compared to the no-wake case. This indicates that the upstream turbine wake has a significant effect on the downstream flow over the downgrade of the gentle hill. However, for the steep hill, the spectrum shown in Fig. 20 indicates that over the whole frequency range, there is no difference between the kinetic energy distributions with and without the effect of the upstream turbine wake. It is believed that the expansion and mixing of the turbulent wake flow is highly restricted by the separated flow induced by the topography. Therefore, the phenomenon of increased kinetic energy in the high-frequency range, which can be clearly found in the gentle hill case, has not been observed in the steep

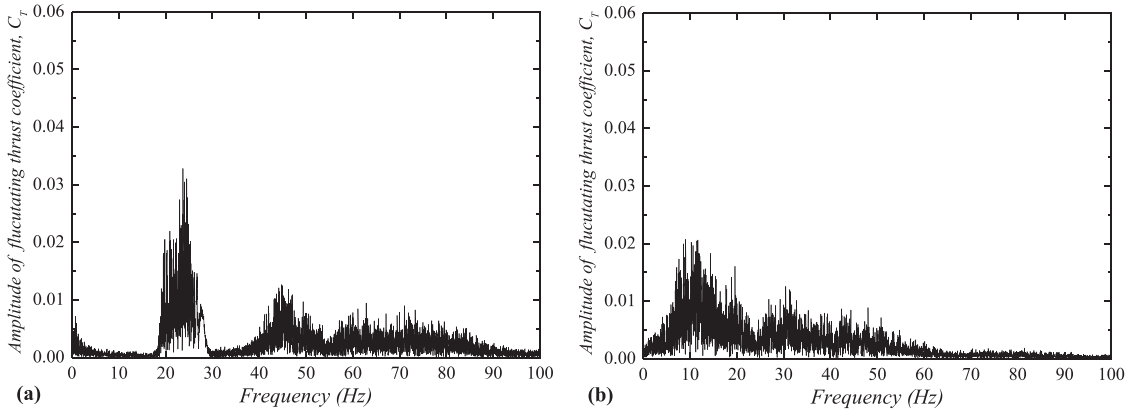

Fig. 17. Power spectra of the instantaneous thrust force. (a) Single turbine sited 6*D* behind the top of the gentle hill (b) Single turbine sited 6*D* behind the top of the steep hill.

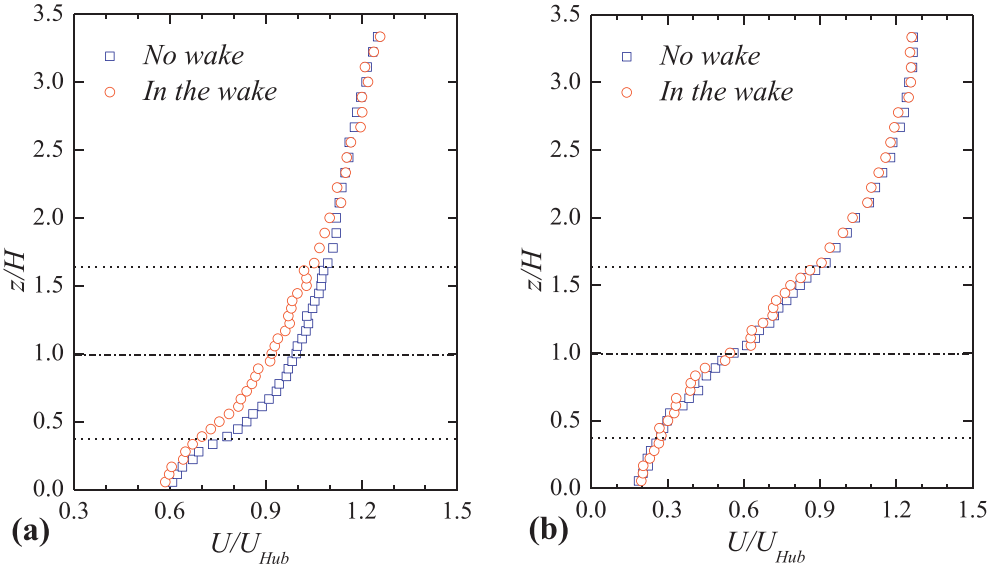

Fig. 18. Comparison of the velocity profiles with and without the effect of upstream turbine wake. (a) Measured 6D behind the top of the gentle hill (b) Measured 6D behind the top of the steep hill.

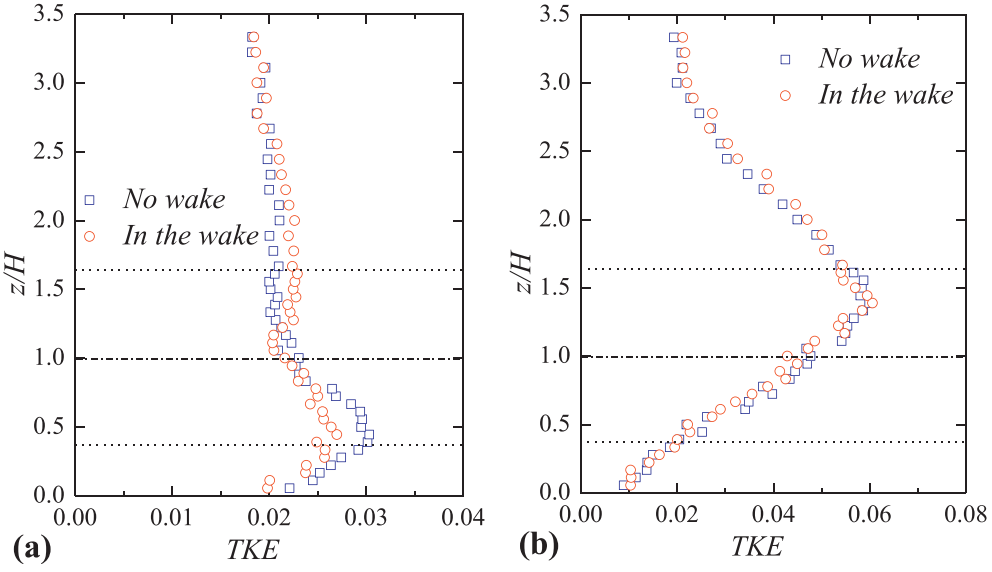

Fig. 19. Comparison of the TKE profiles with and without the effect of upstream turbine wake. (a) Measured 6D behind the top of the gentle hill (b) Measured 6D behind the top of the steep hill.

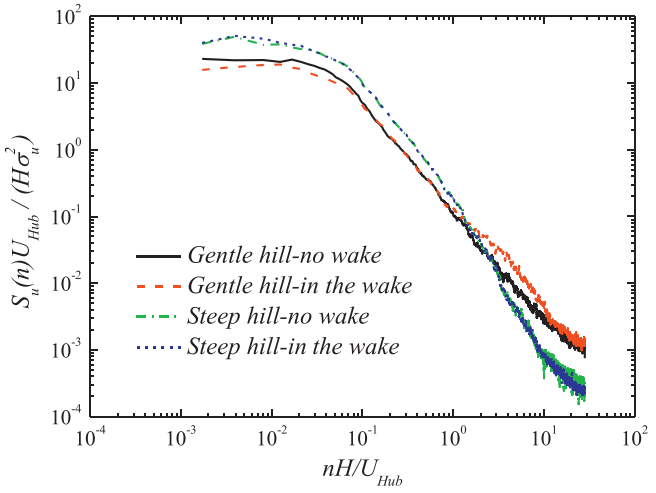

Fig. 20. Spectra comparison of the stream-wise velocity components with and without an upstream turbine mounted on the hilltop (measurement point, *x=6D, (z-H)/D=0.5*).

Table 6
Effect of upstream turbine wake on dynamic wind loads of a wind turbine sited 6*D* behind the hilltop (Using $U_{Hub} = 5\ m/s$ as reference velocity).

Wind load measurement results	Gentle hill		Steep hill	
	No wake	In the wake	No wake	In the wake
Mean thrust coefficient	0.46	0.37	0.16	0.16
The standard deviation of the thrust coefficient	0.28	0.28	0.15	0.15

hill case.

The dynamic wind loads acting on the wind turbines sited 6*D* behind the hilltops with and without the effect of the upstream turbine wake are listed in Table 6. First, while the wind turbine sited on the top of the gentle hill has a significant effect on the mean wind loads acting on the downstream turbine sited 6*D* behind the hilltop (i.e., ~18% decrease in time-averaged thrust force), the change of mean thrust forces corresponding to the steep hill case are almost negligible. Second, the change of the standard deviations of the thrust forces are very small for both the gentle and steep hill cases, which agrees well with the behavior of the TKE distributions shown in Fig. 19.

4. Conclusion

Wind-tunnel experiments were conducted to characterize the aeromechanic performances and wake interferences of wind turbines sited on hilly terrains with different slopes. The dynamic wind loads acting on the model turbines sited on the hilltops and behind the hills were measured and correlated with the flow field measurements to reveal the relationship between the wind turbine performances and the surface wind characteristics for the optimal site design of wind turbines on hilly terrains. The effects of upstream turbine wake on the performances of downstream turbines were also investigated. Some major findings of the present study are summarized as follows:

(1) Compared to the flat surface, the wind turbine sited on the hilltop not only generates more power due to the speed-up effect but also experiences less fatigue loads due to the decreased TKE on the hilltop.
(2) Due to the increase of surface height, the wake effect of the upstream turbine on the wind turbine sited on the hilltop becomes much less significant compared to that on the flat surface. The decreases of mean wind loads caused by the wake of the upstream wind turbines located 6*D* in front of the hilltops are only approximately 4.4% and 2.6% for the gentle and steep hills respectively, which are much lower than that of the flat surface case with the same turbine spacing (i.e., 12%).
(3) The behavior of the dynamic wind loads acting on the wind turbine sited 6*D* behind the hilltop shows obvious differences between the gentle and steep hill cases. Compared to the characteristics of Gaussian distribution for the gentle hill case, the wind turbine located behind the steep hill has a much greater probability to experience extreme wind loads.
(4) While the effect of the upstream turbine wake can be enhanced over the downgrade of the gentle hill, the wake of the wind turbine sited on the top of the steep hill is highly restricted by the separated flow induced by the topography. Compared to the significant wake effect on the mean wind loads acting on the downstream turbine sited behind the gentle hill (i.e., ~18% decrease in mean thrust force), the effect of the upstream turbine wake on the wind turbine sited behind the steep hill is almost negligible.

It should be noted that the topographies investigated in the present study are uniformly shaped two-dimensional hills. Gong and Ibbetson (1989) indicated that for a gentle hill, the mean flow and turbulence over a three-dimensional hill generally resemble those over a two-dimensional hill of similar cross-section. The major differences between two- and three-dimensional hills are found on the upwind slope and in the wake where, respectively, horizontal divergence and convergence of the three-dimensional flow are most pronounced. Ishihara et al. (1999) experimentally studied the turbulent flow over a three-dimensional steep hill. It was found that the pronounced speed-up of flow occurs not only on the hilltop but also at the midway of the sides. In addition, the ABL wind over a three-dimensional steep hill separates behind the crest and reattaches just at the lee foot of the hill, which is quite different from that of the two-dimensional hill. Obviously, these discrepancies of flow characteristics between two- and three-dimensional hills would have a significant effect on the aeromechanic performances of wind turbines. Therefore, a wind tunnel study will be performed in our future work to reveal the aeromechanics and wake interferences of wind turbines sited over typical three-dimensional hills.

Acknowledgement

The funding support from the Iowa Energy Center with Grant No. 14-008-OG and National Science Foundation (NSF) with Grant Numbers of CBET-1133751 and CBET-1438099 are gratefully acknowledged. Wei Tian also wants to thank the support from the National Key Technology Support Program of China (No.2015BAA06B04) and Shanghai Natural Science Foundation (No.16ZR1417600).

References

Adaramola, M.S., Krogstad, P.A., 2011. Experimental investigation of wake effects on wind turbine performance. Renew. Energy 36, 2078–2086.
Architecture Institute of Japan, 1996. AIJ Recommendations for Loads on Buildings. AIJ.
AS/NZ1170.2, 2002. Australian/New Zealand Standard, Structural Design Actions, Part 2: Wind Actions. Standards Australia and Standards New Zealand.
ASCE 7-02, 2002. Minimum Design Loads for Buildings and Other Structures. American Society of Civil Engineers.
ASCE 7-05, 2005. Minimum Design Loads for Buildings and Other Structures. American Society of Civil Engineers.
ASCE 7-10, 2010. Minimum Design Loads for Buildings and Other Structures. American Society of Civil Engineers.
Athanassiadou, M., Castro, I.P., 2001. Neutral flow over a series of rough hills: a laboratory experiment. Bound.-Layer Meteorol. 101, 1–30.
Balogh, M., Parente, A., Benocci, C., 2012. RANS simulation of ABL flow over complex terrains applying an enhanced k – ε model and wall function formulation: implementation and comparison for fluent and openFOAM. J. Wind Eng. Ind. Aerodyn. 104, 360–368.
Barthelmie, R.J., Rathmann, O., Frandsen, S.T., 2007. Modelling and measurements of wakes in large wind farms. J. Phys. Conf. Ser. 75, 012049.

Bechmann, A., Sørensen, N.N., 2011. Hybrid RANS/LES applied to complex terrain. Wind Energy 14, 225–237.
Bitsuamlak, G., Stathopoulos, T., Bédard, C., 2006. Effects of upstream two-dimensional hills on design wind loads: a computational approach. Wind Struct. 9, 37–58.
Bitsuamlak, G.T., Bédard, C., Stathopoulos, T., 2007. Modeling the effect of topography on wind flow using a combined numerical-neural network approach. J. Comput. Civ. Eng. 21, 384–392.
Bowen, A.J., 2003. Modelling of strong wind flows over complex terrain at small geometric scales. J. Wind Eng. Ind. Aerodyn. 91, 859–1871.
Bradley, E.F., 1980. An experimental study of the profile of wind speed, shearing stress and turbulence at the crest of a large hill. Quart. J. Roy. Meteorol. Soc. 106, 101–124.
Britter, R.E., Hunt, J.C.R., Richards, K.J., 1981. Air flow over a two-dimensional hill: studies of velocity speed-up, roughness effects and turbulence. Quart. J. Roy. Meteorol. Sot 107, 91–110.
Cal, R.B., Lebrón, J., Castillo, L., Kang, H.S., Meneveau, C., 2010. Experimental study of the horizontally averaged flow structure in a model wind-turbine array boundary layer. J. Renew. Sustain. Energy 2, 013106.
Cao, S., Tamura, T., 2006. Experimental study on roughness effects on turbulent boundary layer flow over a two-dimensional steep hill. J. Wind Eng. Ind. Aerodyn. 94, 1–19.
Cao, S., Tamura, T., 2007. Effects of roughness blocks on atmospheric boundary layer flow over a two-dimensional low hill with/without sudden roughness change. J. Wind Eng. Ind. Aerodyn. 95, 679–695.
Carpenter, P., Locke, N., 1999. Investigation of wind speeds over multiple two-dimensional hills. J. Wind Eng. Ind. Aerodyn. 83, 109–120.
Chamorro, L., Porte-Agel, F., 2009. A wind-tunnel investigation of wind-turbine wakes: boundary-layer turbulence effects. Bound.-Layer Meteorol. 132, 129–149.
Coppin, P.A., Bradley, E.F., Finnigan, J.J., 1994. Measurements of flow over an elongated ridge and its thermal stability dependence: the mean field. Bound.-Layer Meteorol. 69, 173–199.
Corten, G.P., Schaak, P., Hegberg, T., 2004. Turbine Interaction in Large Offshore Wind Farms: Wind Tunnel Measurements. Energy Research Centre of the Netherlands (ECN). Technical Report No. ECN-C-04–048.
Counihan, J., 1975. Adiabatic atmospheric boundary layers: a review and analysis of data from the period 1880–1972. Atmos. Environ. 9, 871–905.
European Committee for Standardization (CEN), 2004. Eurocode 1: Action on Structures-general Actions-part 1-4: Wind Action (European Standard).
Ferreira, A.D., Lopes, A.M.G., Viegas, D.X., Sousa, A.C.M., 1995. Experimental and numerical simulation of flow around two-dimensional hills. J. Wind Eng. Ind. Aerodyn. 54, 173–181.
Ferreira, A.D., Silva, M.C.G., Viegas, D.X., Lopes, A.G., 1991. Wind tunnel simulation of the flow around two-dimensional hills. J. Wind Eng. Ind. Aerodyn. 38, 109–122.
Finnigan, J.J., Belcher, S.E., 2004. Flow over a hill covered with a plant canopy. Quart. J. Roy. Meteorol. Soc. 130, 1–29.
Flay, R.G.J., Stevenson, D.C., 1998. Integral length scales in strong winds below 20m. J. Wind Eng. Ind. Aerodyn. 28, 21–30.
Gong, W., Ibbetson, A., 1989. A wind tunnel study of turbulent flow over model hills. Bound.-Layer Meteorol. 49, 113–148.
Grant, I., Parkin, P., Wang, X., 1997. Optical vortex tracking studies of a horizontal axis wind turbine in yaw using laser-sheet, flow visualization. Exp. Fluids 23, 513–519.
Haans, W., Sant, T., van Kuik, G., van Bussel, G., 2008. HAWT near-wake aerodynamics, part I: axial flow conditions. Wind Energy 11, 245–264.
Harman, I.N., Finnigan, J.J., 2010. Flow over hills covered by a plant canopy: extension to generalised two-dimensional topography. Bound.-Layer Meteorol. 135, 51–65.
Hu, H., Yang, Z., Sarkar, P., 2012. Dynamic wind loads and wake characteristics of a wind turbine model in an atmospheric boundary layer wind. Exp. Fluids 52, 1277–1294.
Hunt, J.C.R., Leibovich, S., Richards, K.J., 1988a. Turbulent shear flows over low hills. Quart. J. Roy. Meteorol. Soc. 114, 1435–1470.
Hunt, J.C.R., Richards, K.J., Brighton, P.W.M., 1988b. Stably stratified shear flow over low hills. Quart. J. Roy. Meteorol. Soc. 114, 859–886.
Ishihara, T., Hibi, K., Oikawa, S., 1999. A wind tunnel study of turbulent flow over a three-dimensional steep hill. J. Wind Eng. Ind. Aerodyn. 83, 95–107.
Jackson, P.S., Hunt, J.C.R., 1975. Turbulent wind flow over a low hill. Quart. J. Roy. Meteorol. Soc. 101, 929–955.
Jain, P., 2007. Wind Energy Engineering. McGraw Hill. ISBN: 978-0-07-171477-8.
Kaimal, J.C., Wyngaard, J., Izumi, Y., Cote, O.R., 1972. Spectral characteristics of surface-layer turbulence. Quart. J. Roy. Meteorol. Soc. 98, 563–589.
Kim, H.G., Lee, C.M., Lim, H.C., Kyong, N.H., 1997. An experimental and numerical study on the flow over two-dimensional hills. J. Wind Eng. Ind. Aerodyn. 66, 17–33.
Lemelin, D.R., Surry, D., Davenport, A.G., 1988. Simple approximations for wind speed-up over hills. J. Wind Eng. Ind. Aerodyn. 28 (1), 117–127.
Locke, J., Valencia, U., 2004. Design Studies for Twist-coupled Wind Turbine Blades. Sandia National Laboratories. Technical Report No. SAND 2004–0522.
Lubitz, W.D., White, B.R., 2007. Wind-tunnel and field investigation of the effect of local wind direction on speed-up over hills. J. Wind Eng. Ind. Aerodyn. 95, 639–661.
Markfort, C.D., Zhang, W., Porté-Agel, F., 2012. Turbulent flow and scalar transport through and over aligned and staggered wind farms. J. Turbul. 13, 1–36.
Mason, P.J., King, J.C., 1985. Measurements and predictions of flow and turbulence over an isolated hill of moderate slope. Quart. J. Roy. Meteorol. Soc. 111, 617–640.
Mason, P.J., Sykes, R.I., 1979. Flow over an isolated hill of moderate slope. Quart. J. Roy. Meteorol. Soc. 105, 383–395.
Medici, D., Alfredsson, P.H., 2006. Measurements on a wind turbine wake: 3D Effects and bluff body vortex shedding. Wind Energy 9, 219–236.
Miller, C.A., Davenport, A.G., 1998. Guidelines for the calculation of wind speed-ups in complex terrain. J. Wind Eng. Ind. Aerodyn. 74, 189–197.
Panofsky, H.A., Dutton, J.A., 1984. Atmospheric Turbulence-models and Methods for Engineering Applications. John Wiley & Sons, New York.
Paterson, D.A., Holmes, J.D., 1993. Computation of wind flow over topography. J. Wind Eng. Ind. Aerodyn. 46, 471–476.
Pellegrini, C.C., Bodstein, G.C.R., 2004. The height of maximum speed-up in the atmospheric boundary layer flow over low hills. J. Braz. Soc. Mech. Sci. Eng. 26, 249–259.
Politis, E.S., Prospathopoulos, J., Cabezon, D., Hansen, K.S., Chaviaropoulos, P.K., Barthelmie, R.J., 2012. Modeling wake effects in large wind farms in complex terrain: the problem, the methods and the issues. Wind Energy 15, 161–182.
Røkenes, K., Krogstad, P., 2009. Wind tunnel simulation of terrain effects on wind farm siting. Wind Energy 12, 391–410.
Sanderse, B., 2009. Aerodynamics of Wind Turbine Wakes: Literature Review. Energy Research Centre of the Netherlands (ECN). Technical Report No. ECN-E-09–016.
Somers, D.M., 2005. The S819, S820, and S821 Airfoils. National Renewable Energy Laboratory. Technical Report No. NREL/SR-500–36334.
Taylor, P.A., Gent, P.R., 1974. A model of atmospheric boundary layer flow above an isolated two-dimensional hill: an example of flow over gentle topography. Bound.-Layer Meteorol. 7, 349–362.
Taylor, P.A., Walmsley, J.L., Salmon, J.R., 1983. A simple model of neutrally stratified boundary-layer flow over real terrain incorporating wavenumber-dependent scaling. Bound.-Layer Meteorol. 26, 169–189.
Tian, W., Ozbay, A., Hu, H., 2014. Effects of incoming surface wind conditions on the wake characteristics and dynamic wind loads acting on a wind turbine model. Phys. Fluids 26, 125108.
Uchida, T., Ohya, Y., 2003. Large-eddy simulation of turbulent airflow over complex terrain. J. Wind Eng. Ind. Aerodyn. 91, 219–229.
Van Binh, L., Ishihara, T., Van Phuc, P., Fujino, Y., 2008. A peak factor for non-Gaussian response analysis of wind turbine tower. J. Wind Eng. Ind. Aerodyn. 96, 2217–2227.
Vermeer, L.J., Sørensen, J.N., Crespo, A., 2003. Wind turbine wake aerodynamics. Prog. Aerosp. Sci. 39, 467–510.
Walmsley, J.L., Salmon, J.R., Taylor, P.A., 1982. On the application of a model of boundary-layer flow over low hills to real terrain. Bound.-Layer Meteorol. 23, 17–46.
Weng, W., Taylor, P.A., Walmsley, J.L., 2000. Guidelines for airflow over complex terrain: model developments. J. Wind Eng. Ind. Aerodyn. 86, 169–186.
Wilson, R.E., 1994. Aerodynamic behavior of wind turbines. In: Spera, D.A. (Ed.), Wind Turbine Technology: Fundamental Concepts of Wind Turbine Engineering. ASME Press, pp. 215–282.
Ying, R., Canuto, V.M., 1997. Numerical simulation of flow over two-dimensional hills using a second-order turbulence closure model. Bound.-Layer Meteorol. 85, 447–474.
Yuan, W., Tian, W., Ozbay, A., Hu, H., 2014. An experimental study on the effects of relative rotation direction on the wake interferences among tandem wind turbines. Sci. China Phys. Mech. Astron 57, 935–949.
Zhou, Y., Kareem, A., 2002. Definition of wind profiles in ASCE 7. J. Struct. Eng. 128, 1082–1086.